A LIPOSOME-BASED ION RELEASE IMPEDANCE SENSOR FOR HIV DETECTION AT THE POINT-OF-CARE

BY

GREGORY L DAMHORST

THESIS

Submitted in partial fulfillment of the requirements
for the degree of Master of Science in Bioengineering
in the Graduate College of the
University of Illinois at Urbana-Champaign, 2013

Urbana, Illinois

Adviser:

Professor Rashid Bashir

Abstract

Many individuals living in remote and resource-limited regions around the world face a barrier to adequate medical care due to the unavailability of diagnostic instrumentation to perform standard measurements which diagnose disease and inform treatment. Factors which limit the availability of diagnostics include both the costs of instrumentation and per-test costs, inadequate portability, the requirement for a laboratory facility, the time required to perform the test, and a need for highly-trained personnel to operate the instrumentation. While a wide variety of approaches primarily based on innovations in micro- and nanotechnology have been reported toward the point-of-care sensing of biological entities, none has yet emerged as a comprehensive solution to the fundamental problems of diagnostic testing in resource-limited settings. In strides toward a platform for low-cost, rapid, easy-to-use point-of-care diagnostics, we present an ELISA-inspired lab-on-a-chip strategy for biological detection based on liposome tagging and ion-release impedance spectroscopy. Ion-encapsulating dipalmitoylphosphatidylcholine (DPPC) liposomes can be functionalized with antibodies and are stable in deionized water yet become permeable for ion release upon heating, making them ideal reporters for electrical biosensing of surface-immobilized antigens. We demonstrate the quantification of these liposomes by real-time impedance measurements and the detection of HIV, which we have selected as a problem to target in the development of this platform, which ultimately can be applied more broadly to other biomolecules and antigens. By showing the detection of viruses on this biosensor platform, we have demonstrate a proof-of-concept which will be further optimized and advanced toward quantitative determination of viral load from whole blood specimens.

Acknowledgments

I would like to thank Prof. Rashid Bashir for his mentorship, encouragement and for providing the opportunity to do something about which I am passionate. I also thank my colleague Dr. Nicholas Watkins for his mentorship, as well as Eric Salm, Umer Hassan, Maggie Sobieraj, and Jimmy Ni for their contributions to this project. Thanks to MNTL staff, especially Dr. Larry Millet for assistance.

This work is supported in part by the Roy J. Carver Fellowship and the Illinois Distinguished Fellowship in the College of Engineering at the University of Illinois at Urbana-Champaign.

Contents

1. Introduction

Approximately 34 million people worldwide are living with Human Immunodeficiency Virus (HIV), the virus that causes Acquired Immune Deficiency Syndrome (AIDS) [1]. Epidemiological trends reflect recent progress in the expansion of access to prevention, testing, counseling and treatment, including a drop in new HIV infections from 3.1 million annually in 2002 to 2.7 million in 2010 and a decline in AIDS-related deaths from 2.2 million annually in 2006 to 1.8 million in 2010 [1].

These data do not mask the epidemic proportions of the disease, however, and combating HIV/AIDS remains one of eight Millennium Development Goals outlined by the United Nations for reducing extreme poverty [2]. The disease disproportionately affects the world's poorest nations – for example, 68% of all people living with HIV reside in Sub-Saharan Africa, a region that represents only 12% of the global population [1]. Because of the absence of an effective vaccine, the availability of antiretroviral medications and accessibility of testing represent the most significant grand challenges in fighting the HIV/AIDS epidemic worldwide. These two challenges do not stand independently, however, as regular and appropriate monitoring is required for effective treatment.

HIV infection is typically diagnosed by serologic tests indicating the presence of anti-HIV antibodies, a test for which rapid point-of-care assays are available including tests of oral fluids and whole blood from a finger prick [3]. Following diagnosis, guidelines issued by the Infectious Disease Society of America (IDSA) recommend immediate evaluation of two core markers of the progress of infection: the CD4+ T lymphocyte count and plasma viral load, in addition to antiretroviral therapy (ART) resistance testing, a complete blood count, and blood chemistry panels [3]. Typical levels of CD4+ T lymphocytes and plasma viral load during the course of HIV infection are depicted in Fig. 1 [4], [5]. World Health Organization (WHO) guidelines recommend the initiation of ART for people living with HIV upon determination of a CD4 count less than or equal to 350 cells/mm^3, while CD4 count monitoring is recommended to be performed at least every six months for individuals not yet eligible for ART [6]. During treatment, the WHO recommends CD4 counting and viral load monitoring in a routine approach [6]. Ultimately, the goal of regular monitoring is to guide treatment strategies toward the prevention of immunological failure (CD4 count below baseline, 50% of on-treatment peak value, or 100 cells/mm^3), and virological failure (viral load above 5000 copies/ml) [6].

The CD4 count reflects the health of the immune system and is occasionally paired with the CD8+ T lymphocyte count in assessment of an HIV-positive patient, although there are conflicting reports on the utility of CD8 counts or CD4/CD8 ratio [3], [7]. Viral load measurements complement the CD4 count and are a direct assessment of viral number. Viral load is typically assessed by quantifying viral RNA in

This text originally appeared in Damhorst GL, Watkins NN, Bashir R, "Micro and nanotechnology for HIV/AIDS diagnostics in resource-limited settings," IEEE Trans Biomed Eng. 2013 Mar;60(3):715-26. doi: 10.1109/TBME.2013.2244894.

the blood plasma, although alternative approaches to quantifying plasma load as well as intracellular viral reservoirs have been described. A review of the HIV lifecycle in Fig. 2 reveals several traditional and alternative biomarkers for monitoring virus levels.

Because of retrovirus integration with the host in the form of a provirus, HIV establishes a long-term reservoir and accomplishes production of new virions in host cells – a process which can be interrogated at all levels of gene expression inside the cell. Detection of proviral DNA is the most commonly assessed intracellular marker and has established clinical relevance as a method for assessing virus status in newborns in whom mother-to-child transmission of HIV is suspected, since passive transfer of maternal antibodies can produce false-positives on serological tests [3]. However, assessment of levels of cell-associated unspliced and multiply-spliced HIV RNA have also been suggested as clinical markers of disease progression [8–10], to have prognostic value [11], or to be useful metrics for assessing ART efficacy [12], [13]. Laboratory-based methods for the detection of cell-associated RNA have been demonstrated [14], [15].

The core principles of micro- and nanotechnology offer opportunities for new approaches to monitoring all of these biomarkers. Modern fabrication techniques have enabled the development of novel optical, mechanical and electrical biosensor platforms with greater sensitivity for cell and biomolecule sensing, including those which replace or eliminate the need for expensive and bulky components of state-of-the-art clinical diagnostic instruments. Microfluidic systems enable precise manipulation of small volumes of biological fluids, significantly decreasing blood sample size requirements and allowing for less invasive collection techniques. Finally, smaller instrument footprints promise a high degree of portability in sample-to-answer systems.

This review emphasizes approaches toward the implementation of technologies for CD4 T lymphocyte counting, plasma viral load and proviral load determination in resource-limited settings. Approaches vary from adaptations of state-of-the art technologies to novel assays based on innovations in micro- and nanotechnologies. Several technologies discussed here address testing challenges through complete sample-to-answer integrated systems while others demonstrate partial solutions, yet demonstrate potential for application in an integrated system.

In addition to the typical requirements for sensitivity and specificity required of diagnostic technologies, the criteria for effective CD4 counting or viral load determination in resource-limited settings includes: (1) the test must be able to operate at the point-of-care, addressing the need to bring testing to patients with limited ability to travel to a healthcare facility, (2) the test must be rapid, addressing complications in resource-limited settings associated with healthcare provider follow-up when results cannot be obtained same-day, (3) the test must be low-cost, mitigating the financial burden on individuals, agencies or governments in poor countries, and (4) the test must be easy to use, allowing for

implementation in areas where skilled technicians are not available. The end goal is a comprehensive technology capable of taking whole blood input in the form of a finger-prick or heel-prick, and outputting the desired results.

Figures

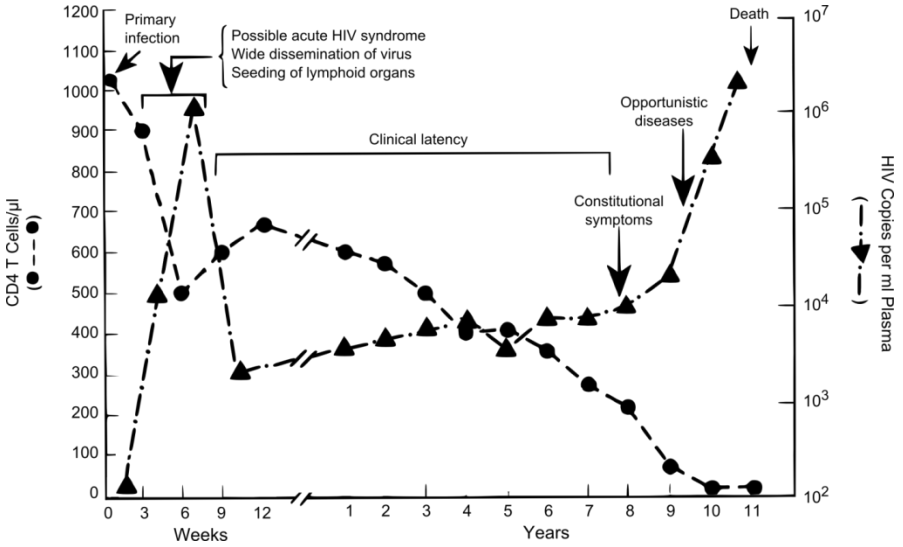

Fig. 1. Typical course of infection. Typical CD4 counts and plasma viral load during the course of an HIV infection. Adapted from [4], [5].

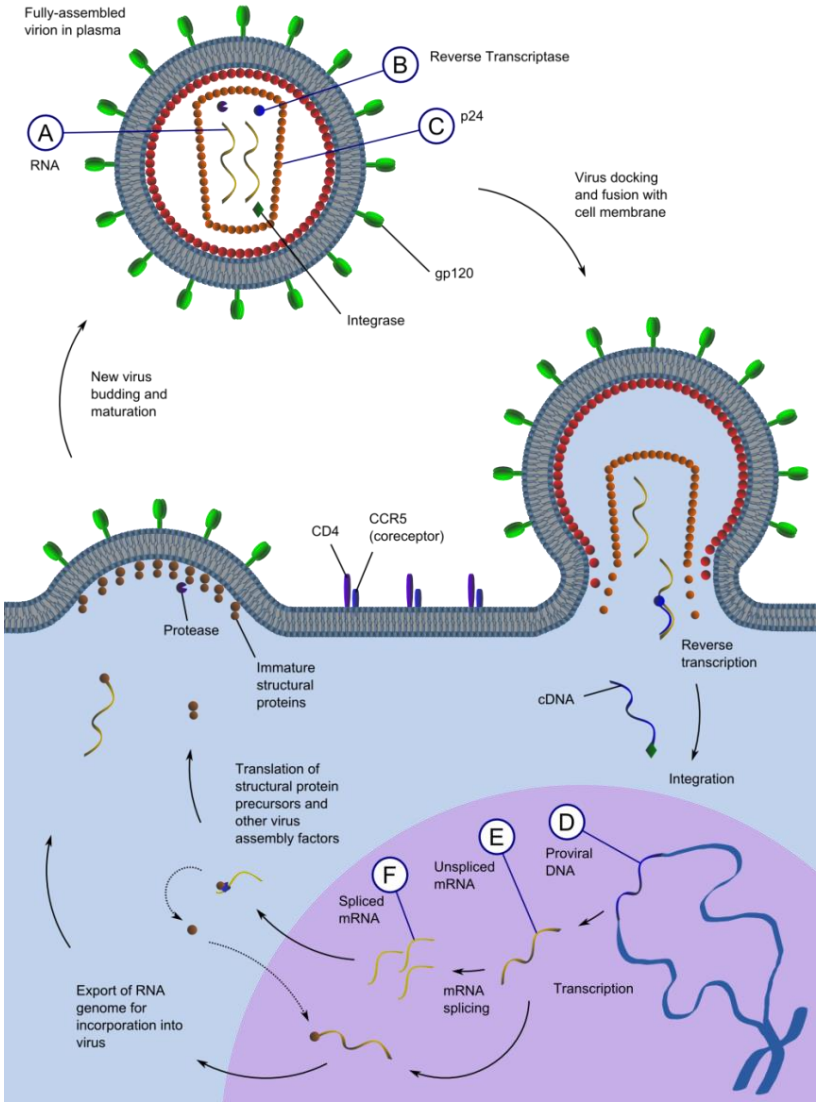

Fig. 2. HIV lifecycle showing critical points for virus detection. Virions in plasma infect CD4+ T lymphocytes via the high-affinity interaction between the viral surface protein gp120 and the host cell CD4 receptor and CCR5 co-receptor. This docking facilitates fusion of the viral and cell membranes and injection the protein capsid into the cytoplasm which dissociates to release viral RNA. Highly error-prone reverse transcriptase makes a cDNA copy of the viral genome which is targeted to the host cell nucleus and integrated with the host genome by viral protein integrase. Host cell gene expression including mRNA alternative splicing ensues, resulting in expression of both viral structural protein precursors and those involved in the facilitation of viral gene expression. Genomic RNA and structural proteins are targeted to the cell surface where budding occurs. Maturation facilitated by protease action takes place after budding. Labels indicate biomarkers for viral diagnostics, including (A) Viral RNA in plasma (B) Reverse Transcriptase in plasma (C) Capsid protein p24 in plasma (D) Proviral DNA (E) Cell-associated unspliced RNA (F) Cell-associated spliced RNA.

2. Literature Review

2.1 Plasma Viral Load

2.1.1 Current State of the Art

Several challenges complicate the monitoring of HIV plasma viral load, including the diversity of HIV forms and subtypes as the result of high recombination and mutation rates – one of the primary barriers to the development of an effective vaccine [16]. Effective viral load devices must therefore be capable of flexibility among genetic or antigenic variation from infection to infection.

State of the art technology for plasma viral load involves amplification and detection of viral nucleic acid. Tests approved by the U.S. Food and Drug Administration for quantification of plasma viral load by nucleic acid amplification are listed in Table 1 [17–20]. To date, however, no Reverse-Transcription Polymerase Chain Reaction (RT-PCR), branched DNA (bDNA), or Nucleic Acid Sequence-Based Amplification (NASBA) assay has demonstrated the qualities necessary to become ubiquitous in resource-limited settings.

Multiple studies have also explored the possibility of transporting dried blood or plasma specimens from more primitive sites to a capable laboratory as a global health solution for plasma viral load testing, though this does not address the ultimate need for a rapid, point-of-care test [21–24]. Progress toward viral load in resource-limited settings has emerged in the form of assays for other biomolecular components of HIV, including the structural capsid protein p24 and the enzyme reverse transcriptase, platforms aimed at the miniaturization of the amplification and/or detection aspects of nucleic acid quantification, and isolation of whole viruses from blood samples as a processing step toward direct particle counting. Several novel non-quantitative technologies for detection of HIV in plasma have been reported, including a recent report from De la Rica and Stevens on a gold-nanoparticle-based p24 assay that can be analyzed with the naked eye [25]. Non-quantitative techniques are only presented extensively in this section, however, when considered relevant to the development of a future quantitative technique.

2.1.2 Global Health Solutions

2.1.2.1 Detection of p24 capsid proteins

The Enzyme-Linked ImmunoSorbent Assay (ELISA) is a standard technique for laboratory detection and quantification of proteins. P24 assays developed by Perkin Elmer Life Sciences (Boston, MA) [26–29], NEN Life Science Products (Geneva, Switzerland) [30], and Biocentric (Bandol, France) [31] have been evaluated for use in resource limited settings but sensitivity [27], reliability [27], [30] and false positives [31] have been cited as reasons limiting implementation of these tests in resource-limited

This text originally appeared in Damhorst GL, Watkins NN, Bashir R, "Micro and nanotechnology for HIV/AIDS diagnostics in resource-limited settings," IEEE Trans Biomed Eng. 2013 Mar;60(3):715-26. doi: 10.1109/TBME.2013.2244894.

settings. Alternative assays have been developed, however, for the detection of p24 as the basis for HIV quantification [32–36].

Lee, et al. sought to improve upon the standard ELISA with a nanoarray patterned with anti-p24 antibodies by dip-pen nanolithography [32]. Instead of an enzyme with chemiluminescent product, a gold nanoparticle probe functionalized with anti-p24 antibody was used as a secondary tag and detected with atomic force microscopy and scanning electron microscopy. While this report serves as an interesting proof-of-concept, a more appropriate detection technique is necessary as these microscopy techniques are probably not suited for low-cost, portable applications.

Parpia, et al. described a dipstick assay for p24 designed for rapid detection of HIV in infants [33]. Plasma samples were mixed with heat shock buffer, heated to disrupt immune complexes, and then exposed to the dipstick test. The sample hydrates an antibody-conjugated tag and flows laterally by capillarity to a test line where antigen-bound tags are immobilized. The dipstick is then scanned and analyzed by a computer for semi-quantitative results. This technique makes strides toward the ideal platform for point-of-care viral load determination, although integrated scanning and analysis may be necessary to achieve the desired ease-of-use.

The concept of a biobarcode detection assay was introduced by Nam, Thaxton and Mirkin in Science in 2003 [37]. The technique was later adapted for detection of HIV capsid protein p24 [34–36] and an overview of the concept is depicted in Fig. 3 [34]. The biobarcode assay is a modification of traditional ELISA techniques in which p24 is first captured in microtiter wells coated with anti-p24 antibody and subsequently tagged with a biotinylated anti-p24 [34]. Streptavidin-coated gold nanoparticles are then bound to the secondary antibody, providing a substrate for attachment of biotinylated barcode DNA. Following washing and heating, biobarcode DNA immobilized on gold nanoparticles bound to p24-antibody sandwiches is eluted and hybridized to a sequence complementary to half of the barcode DNA on a glass slide. A DNA-probe labeled gold nanoparticle binds to the other half of the immobilized barcode DNA and silver ions are reduced by hydroquinone on the surface, amplifying the visualization of biobarcode signals. A later version of this assay replaced the microtiter wells with antibody-coated magnetic nanoparticles which facilitated the separation of the antigen-nanoparticle complexes from solution [36]. This biobacode technique has demonstrated promising strides toward the grand challenge of early HIV detection [35] and bears the potential for a quantitative test, yet it has not yet been shown as a suitable replacement for quantitative nucleic acid detection technologies or to have been evaluated for efficacy in resource-limited settings.

2.1.2.2 Detection of reverse transcriptase activity

Reverse transcriptase (RT) is an essential component of replication-competent HIV and thus a specific marker of HIV infection. The ExaVir™ Load assay (Cavidi Tech AB, Uppsala, Sweden), which

is based on the detection of RT activity, was first described by Ekstrand, et al. [38]. This assay requires pre-treatment of blood plasma from HIV-positive blood and isolation of the virus on an immobilization gel column with subsequent washing to remove anti-RT antibodies or RT-inhibiting antiretroviral drugs which are present in many individuals undergoing ART [39], [40]. The sample is eluted from the immobilization column by washing with a viral lysis buffer that frees virus-encapsulated RT for assay. RT activity is quantified based on incorporation of 5-bromodeoxyuridine 5' triphosphate (BrdUTP) in RT DNA product and subsequent BrdUTP tagging with an alkaline phosphate-conjugated antibody. A substrate for AP is then introduced after washing for colorimetric or fluorimetric analysis. The ExaVir™ assays have been evaluated for sensitivity, practicality and flexibility among various HIV subtypes by several clinical studies, including investigations in Burkina Faso [41], Mobmasa, Kenya [31], Botswana [42], Nairobi, Kenya [43], and Johannesburg, South Africa [27]. Evaluations appear optimistic toward the potential of the ExaVir™ as a less-expensive alternative to PCR [26], [27], [31], [41–49].

2.1.2.3. Miniaturization of PCR, non-quantitative

Several efforts to adapt state-of-the-art testing for resource limited settings has involved simplification or automation of various aspects of PCR. For example, Tang et al. developed an isothermal amplification kit based on a reverse-transcriptase helicase-dependent nucleic acid amplification technique which was integrated with a vertical-flow DNA detection strip [50]. The assay, however, still required rigorous preparation of the sample in a laboratory setting, including the purification of viral RNA. Lee et al. described an isothermal simple amplification-based assay (SAMBA) that could be performed on a table-top point-of-care machine including both amplification and dipstick detection [51].

Lee, Kim, Kang and Ahn developed a microfluidic design for on-chip RT-PCR containing mixture and reaction chambers for reverse transcription and PCR as well as a detection chamber in which amplified product is immobilized on complementary probe DNA [52]. An overview of their microfluidic PCR device is depicted in Fig. 4 [52]. An infrared lamp serves as the heart source for PCR thermo cycling and immobilized amplified PCR product is tagged with horseradish peroxidase which reacts with substrate solution to produce a chemiluminescent product for optical detection. This lab-on-a-chip design was capable of performing RT-PCR in 35 minutes, but requires further demonstration of sufficient sensitivity and has not been analyzed for quantitative detection.

2.1.2.4. Miniaturization of PCR, quantitative

Shen, et al. described the application of a SlipChip device to amplification of HIV RNA [53]. RT-PCR mixture containing samples is introduced to 160 wells each of 1 nL, 5 nL, 25 nL and 125 nL allowing for multiplexed analysis. Correct volumes are ensured by dead-end filling facilitated by rotational slipping of a layer of the chip and digital PCR is performed, allowing quantification of viral RNA copies. Digital PCR fluorescence on the SlipChip is demonstrated in Fig. 5 [53]. Ultimately, the

technique was capable of detecting 37 viral copies per ml plasma although additional demonstration of this approach is necessary for consideration as a platform for field testing.

Rohrman, et al. recently described another gold nanoparticle-based technique for the detection of amplified HIV RNA [54]. In their study, NASBA product is placed on a conjugate pad containing gold nanoparticles functionalized with complementary RNA strands which bind the sequence of interest. The sample flows laterally by capillarity down a nitrocellulose membrane strip to a detection zone in which nanoparticle-bound sequences are immobilized. An enhancement solution reduces metallic ions on the surface to increase the colorimetric result, which can be assessed with a common cell phone camera. The assay is paper-based and is easily destroyed by incineration and is reported to cost approximately $0.80 per strip, however it relies on amplified nucleic acid and thus does not present a solution to some of the most fundamental challenges to implementing PCR-based technologies in resource-limited settings.

Tanriverdi, et al. adapted a commercially available HIV assay to fit a portable, fully integrated and automated diagnostic system called Liat Analyzer [55]. 200 µl plasma is loaded into an assay tube and loaded into the analyzer which prepares the sample by performing viral lysis and nucleic acid conjugation with magnetic glass beads. The analyzer elutes the viral RNA and performs reverse transcription and PCR with real-time fluorescence detection, showing good correlation with COBAS TaqMan HIV-1 and Versant HIV-1 RNA (bDNA) assays. The full process is depicted in Fig. 6 [55]. The fully-integrated test is completed in 88 minutes and exhibits a limit of detection of 1,000 copies/ml, leaving room for improvement to compete with the most rapid and sensitive technologies.

2.1.2.5. Virus isolation

In strides toward alternative (non-PCR) approaches to HIV quantification, direct capture of HIV in microfluidic flow-through devices has been demonstrated by Demirci, et al. [56–58]. Briefly, a microfluidic chamber is functionalized with antibodies specific for the HIV envelope-associated protein gp-120 through a variety of surface chemistry techniques and 10 µl [56], [57] or 100 µl [58] of whole blood containing HIV was flowed through the device. Captured viruses were initially visualized with quantum dot tags to verify capture [56], [57], but in a more recent report were lysed on-chip, collected, and interrogated by RT-qPCR for HIV nucleic acid showing 69.7-87.6% capture efficiency for a variety of subtypes and viral loads [58].

In another approach, Chen, et al. mixed virus-containing plasma with superparamagnetic nanoparticles functionalized with anti-CD44, an antibody that binds HIV, and injected the sample onto a microfluidic chip with geometries designed for mixing [59]. Ferromagnetic particles in the fluidic device concentrate an external magnetic field that concentrates virus-bound particles, achieving separation from plasma. Isolated sample is then lysed and interrogated for p24 with an ELISA kit, revealing a maximum capture efficiency of 79% [59]. An overview of this capture device is shown in Fig. 7 [59]. These

platforms, which ultimately could be integrated in a sample-to-answer system, create the opportunity for improved sensitivity by removing the virus from whole blood or plasma and thereby eliminating contaminants which may interfere with detection.

2.2 Proviral Load

2.2.1 Current State of the Art

Provirus refers to the genome of a virus directly integrated with the DNA of the host cell. The proviral load is not as ubiquitous as the plasma viral load or CD4+ T lymphocyte count in clinical management of HIV/AIDS, yet it bears certain significance as the standard for early diagnosis of infection in newborns for whom mother-to-child transmission is suspected, since serological testing is inadequate due to the possibility of false positives from the presence of passively acquired maternal antibodies [3], [60–66]Many have also acknowledged that the proviral load may be an opportunity for early detection in adults in the 2-8 week window period [67] before seroconversion [61–63], a useful alternative for monitoring of ART when plasma RNA levels are undetectable [61], [68], [69], or a complement to the plasma RNA load for diagnostic or prognostic purposes [61], [68], [70–73]. Laboratory techniques for detection of proviral DNA that have been described including non-quantitative PCR approaches [64], [74], quantitative PCR approaches [14], [61], [68], [69], [75], [76], electrochemiluminescence-based detection of PCR products [62], enzyme immunoassay detection of PCR products [63], and one study which performed PCR analysis on dried blood spots [60].

2.2.2 Global Health Solutions

Jangam, et al. presented a solution to the challenges of sample preparation in resource-limited settings when analyzing proviral load with a low-cost extraction technique called filtration isolation of nucleic acids (FINA) [77]. In this technique, whole blood is introduced on a membrane disk and subsequently washed with NaOH resulting in isolation of genomic DNA on the membrane. The membrane is then placed directly in a PCR reaction mix for quantitative analysis. Recently, the same group has reported integration of this extraction method with a sample-to-answer point-of-care PCR system for proviral DNA detection [78]. In this case, blood collected from a heel prick is lysed in the blood collection device, applied to a separator module for FINA, and inserted into an injection-molded assay card. The assay card contains reagents for PCR prepackaged in a foil laminate reagent reservoir and the entire card it inserted directly into a table-top instrument which performs reagent delivery, thermal cycling and fluorescence detection. The estimated cost of the instrumentation is $3,000.00 while each disposable assay card is expected to cost $50.00 or less, a per-test cost on the higher end of the range of estimates reported in the approaches discussed in this review.

Wang, et al. have also recently described a device capable of proviral DNA detection on a chip [79]. In this proof-of-concept, HIV-infected T cells were loaded onto the chip where they were first heat-lysed

and then hybridized with nucleotide probe-conjugated magnetic beads. A permanent magnet was then used to immobilize probes while debris was cleared with a vacuum and the sample was washed. Purified sample was then split between four separate chambers containing unique primer pairs, and PCR amplification was performed and monitored by SYBR Green I fluorescence and integrated optical detection. The whole process was completed in 95 minutes, demonstrating potential for implementation as a point-of-care device in resource-limited settings, although demonstration of this technique from whole-blood input would be necessary for truly point-of-care applications.

2.3 CD4+ T Lymphocyte Count

2.3.1 Current State of the Art

The current gold standard for enumeration of CD4+ T lymphocytes involves immune-staining and analysis of cells with a flow cytometer, a technique that not only requires expensive and bulky instrumentation but also highly-trained laboratory technicians. In efforts to bring CD4 enumeration to resource-limited settings, various techniques have been employed. Here we organize various technologies for CD4 enumeration in resource-limited settings based on the following categories: optical detection methods, electrical detection methods, technologies based on microcytometry employing either optical or electrical techniques, catch-and-release devices, and instrument-free methods.

2.3.2 Global Health Solutions

2.3.2.1 Optical methods

Many efforts have used fluorescent tagging and subsequent image processing to automatically enumerate CD4+ T lymphocytes in micro chambers. Some designs relied on the even distribution of cells in a plastic chamber to produce accurate counts [80]. Others have used a micro fabricated membrane to filter out erythrocytes, leaving leukocytes, which were fluorescently labeled [81]. Specialized image processing algorithms have been developed for the analysis of images from such devices [82]. Thorslund et al. developed and refined a bio-activated PDMS device for capture of CD4+ cells and subsequent imaging with HOECHST and CD3-FITC [83], [84].

Fluorescence detection was later enhanced by using quantum dots [85], [86], forming the technology behind LabNow, Inc. Another approach used immuno-specific paramagnetic beads to bring fluorescently labeled CD4+ T cells into the focusing plane for analysis, reducing counting error [87–89]. Cheng et al. have investigated CD4+ T cell capture by controlling shear stresses at the chamber walls and enumerating cells using a cocktail of fluorescently labeled antibodies [90], [91]. They improved their design by including a monocyte depletion chamber to reduce the positive bias created at lower CD4+ T cell concentrations [92].

Beck et al. have eliminated the off-chip labeling step required by the aforementioned methods by coating capture chambers with hydrogels containing fluorescent antibodies and drying them for storage

[93]. During testing, blood enters the capture region, causing the hydrogel to swell and release the antibodies, specifically labeling CD4+ and CD8+ T cells. Subsequent fluorescent image cytometry is used to obtain the CD4+ and CD8+ T cell counts. The Alere Pima CD4 counter uses a similar method to label CD4+ T cells using cartridges containing a lyophilized antibody pellet [93], [94], and has shown some success in field testing including sites in Harare, Zimbabwe [95], Maputo, Mozambique [96], Gauteng Province, South Africa [97], Kampala, Uganda [98] and London, UK [99]. However, in some situations, it has operational costs similar to or more expensive than standard lab flow cytometric analysis [97], [100].

The aforementioned optical methods require the use of lenses and focusing to analyze samples, but this can increase the cost and decrease the portability of the device and several technologies have made attempts at simplifying the optical component. Gohring et al. quantified the antibody-mediated attachment of T cells by the amount of shift in the whispering gallery mode of an optofluidic ring resonator [101]. Moon et al. counted immobilized helper T cells by their shadows cast over a charge coupled device (CCD) by a white light source [102], [103]. Wang et al. further simplified the optics by not requiring an external light source: immobilized CD4+ T cells were labeled with CD3-conjugated horseradish peroxidase to facilitate a chemiluminescent reaction, which was amplified and quantified by a photodetector [104]. This device was tested using samples from patients at a treatment center in Dar es Salaam, Tanzania [105].

2.3.2.2 Electrical methods

Electrical methods for enumerating CD4+ T lymphocytes are promising due to the fact that they would not require optical components such as lenses, filters, light sources, photodetectors, and CCDs, which can be expensive, bulky, fragile, and require periodic maintenance. An electrical PoC solution could require only solid state components to electrically interrogate a sensing geometry, process sensor output, and provide input from and results to the user.

Mishra et al. used three-electrode cyclic voltammetry to estimate the number of CD4+ T cells that were selectively captured on a working electrode [106], [107]. Jiang et al. have used this design as a building block to create an array of 200 of these electrochemical sensing regions, or pixels, conjugated with CD4 antibody. A pixel would be considered on when a CD4+ T cell was captured, and a total cell count was the total number of on pixels [108].

Cheng et al. enhanced their CD4+ T cell capture device ([90], [91]) by integrating impedance spectroscopy sensing into the capture channel to monitor cell lysate [109]. T cells from whole blood were captured on-chip and lysed in a low-conductivity buffer, releasing intracellular ions into the bulk solution, thereby changing its conductance, which increased proportionally with cell concentration. Impedance-phase spectra and correlation with cell concentration are shown in Fig. 8 [109]. The authors were able to

correlate cell concentration with channel conductance with a detection sensitivity of 20 cells/uL, eliminating the need of a microscope and manual cell counting. Daktari Diagnostics, Inc., has developed the Daktari CD4 counting platform based on this technology.

The lysate impedance method has shown to be an extremely promising technology to penetrate into resource poor regions, as it requires no off-chip sample preparation, employs an electrical interrogation method, and is simple to operate. However, inherent drawbacks from measuring lysate impedance may reduce its efficacy. This technology assumes that T cells from various individuals contain similar ion concentrations, which may not be true, resulting in counting error. In addition, since the technology is sensitive to the concentration of ions, contamination from the sensor chip's materials and failure to wash away excess ions may reduce the system's counting resolution and dynamic range.

2.3.2.3 Microcytometer approach

Kiesel et al. worked toward the goal of a compact flow cytometer with a spatial modulation technique for CD4 identification [110]. Wang et al. have developed a microfluidic chip which first labels CD4+ and CD8+ T lymphocytes (from buffy coat samples) on-chip using pneumatic vortexing before hydrodynamically focusing and laser-induced fluorescence (LIF) counting [111]. They were able to produce CD4/CD8 T cell ratios similar to that found using standard flow cytometry. Yun et al. developed a microfluidic flow cytometer enhanced by FITC-doped silica nanoparticles that required only a single detector [112]. Mao et al. designed a microfluidic flow cytometer with three-dimensional hydrodynamic focusing of CD4+ T lymphocytes and LIF detection [113].

Wang et al. integrated a commercial metal oxide semiconductor field effect transistor (MOSFET) with optical fluorescence detection to determine the percent of CD4+ T cells among a total population of lymphocytes [114]. They have also created a similar system replacing the MOSFET with a two-stage differential amplification system [115], [116]. However, the added complexity of integrating both electrical and optical measurement systems may be prohibitive for PoC applications.

Holmes et al. have developed an electrical microcytometer that can differentiate between different leukocyte subtypes, such as lymphocytes, monocytes, and neutrophils, solely on their impedance characteristics at two different frequencies, as depicted in Fig. 9 [117], [118]. They were subsequently able to enhance electrical differentiation of CD4+ T cells from other leukocytes by specifically attaching 2.2 μm CD4 antibody conjugated latex beads to the T cells to modify their high and low frequency characteristics [119]. They showed good correlation between their electrical chip-based method and the flow cytometry standard for the percentages of CD4+ T cells in white blood cell populations. However, the off-chip bead labeling steps they used would need to be integrated into the chip itself for this technology to be practical in resource-poor applications – a task that is difficult to perform in the laminar flow regime found at the microscale.

Watkins, et al. developed an impedance-based microcytometer for determining CD4 T cell counts employing a resistive pulse technique [120]. Cells were initially focused in a three-dimensional flow sheath for one-by-one flow past a pair of coplanar electrodes and subsequent analysis of AC impedance indicated cell passage by a impedance pulse. A coplanar three-electrode configuration was implemented in a later device which incorporated entrance and exit counting as white blood cells were passed through an anti-CD4 antibody-functionalized capture chamber as illustrated in Fig. 10 [121]. CD4+ T cells were depleted from the sample by immobilization in the capture chamber and the absolute CD4 count was provided by the difference between entrance and exit counts.

2.3.2.4 Catch-and-release

Chemical release of CD4+ T cells post capture has proven to be more difficult, as the cells may further bond to the substrate nonspecifically through membrane adhesion molecules. Zhu et al. have shown the capture and release of CD4+ T cells using electrochemical reactions on microfabricated electrodes; however some drawbacks are that some cell death occurs after T cell release (~10%) and agitation is needed to assist in electrochemical desorption, which is more difficult in the laminar flow regime found in a closed microfluidic chamber [122], [123]. In addition, mass production may be hindered by the fact that the capture region is limited to the area defined by the electrodes, requiring a PEG gel passivation layer elsewhere to prevent non-specific cell capture.

Gurkan et al. used a temperature responsive polymer to capture and release CD4+ T cells [124]. A capture chamber coated with poly(N-isopropylacrylamide) (PNIPAAm) was immobilized with CD4 antibody-Neutravidin complexes at 37 degrees C – when the polymer is hydrophobic and prefers interactions with the Neutravidin. CD4+ T cells are captured at the same temperature before washing away unbound cells and lysing erythrocytes. The CD4+ T cells are released by decreasing the chip's temperature below 32 degrees C, when the PNIPAAm layer becomes hydrophilic, releasing the antibody-Neutravidin complexes and thereby releasing the CD4+ T cells. They were able to release 59% of captured CD4+ T cells with high viability (94%). This method needs to address a few challenges before being a practical PoC device. This includes ensuring surface chemistry is preserved from manufacture to test (i.e., storing the chips at ~37 deg C) and improving the release efficiency for accurate CD4+ T cell enumeration.

2.3.2.5 Instrument-free methods

Since 2005, the Bill and Melinda Gates Foundation has been funding a CD4 initiative (centered at Imperial College London) to create simple, power-free CD4+ T cell counting technologies that would lessen costs and increase penetration into resource-poor regions [125]. A semiquantitative immunochromatographic strip (ICS) being developed by The Burnet Institute compares the intensity of gold particles that are specifically attached to CD4+ T cells at a CD4 capture strip to a reference strip

which has a similar intensity to a known concentration of CD4+ T cells [126]. Zyomyx has developed a device that uses the sedimentation of high density CD4 antibody-conjugated beads to estimate the concentration of CD4+ T cells from whole blood samples [126], [127]. These beads specifically attach to the CD4+ T cells and are sedimented with the help of a manually powered centrifuge. The height of sedimentation in the column is proportional to the concentration of CD4+ T cells, and is viewed through a window and compared to calibrated markings to give the CD4+ T cell count. The device also contains a chamber which used CD14-conjugated magnetic particles and a magnetic collar to deplete monocytes before the sedimentation step. These semi-quantitative instrument-free methods may be viewed as short-term solutions, but fully-quantitative micro- and nanotechnology solutions promise more precise and user-friendly approaches.

Tables

Table 1. FDA-approved tests for plasma viral load quantification

Test name [17–19]	Manufacturer	FDA Approval [18], [20]	Type
Roche Amplicor HIV-1 Monitor Test	Rochem Molecular Systems, Inc.	3/2/1999	RT-PCR
NucliSens HIV-1 QT	bioMerieux, Inc.	11/19/2001	NASBA
VERSANT HIV-1 RNA 3.0 Assay (bDNA)	Bayer Corporation, Berkeley, CA	9/11/2002	bDNA
Abbott RealTime HIV-1 Amplification Kit	Abbott Molecular, Inc.	5/11/2007	RT-PCR
COBAS TaqMan HIV-1 Test	Roche Molecular Systems, Inc.	5/11/2007	RT-PCR

Figures

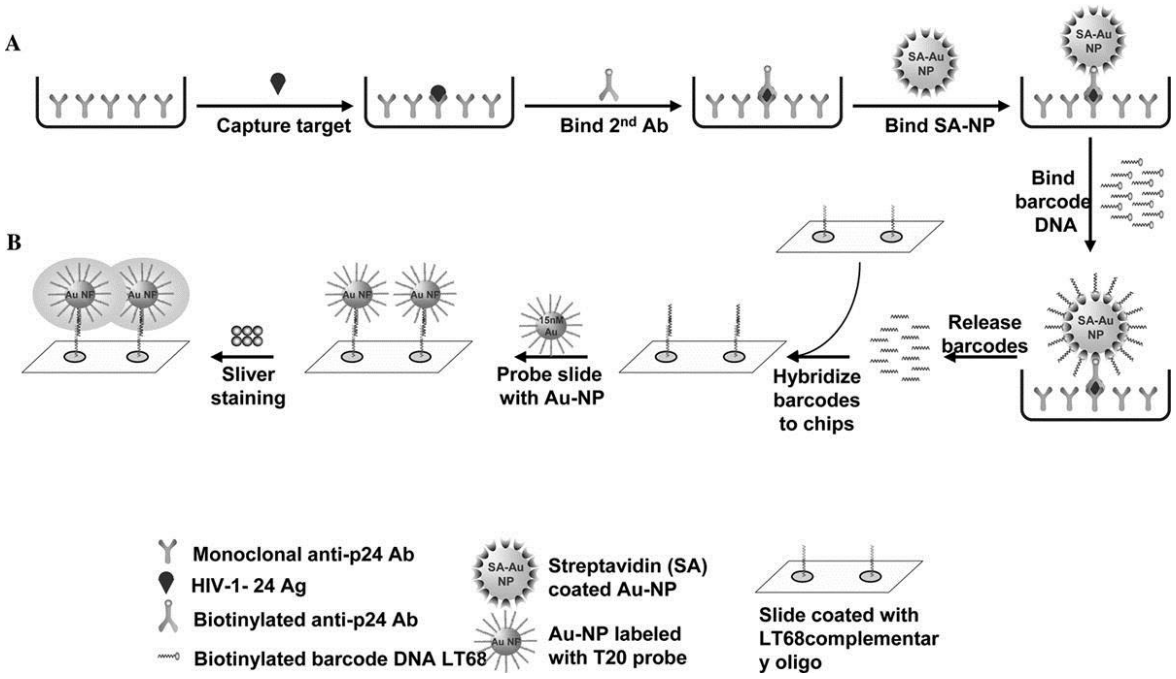

Fig. 3. Biobarcode assay for the detection of HIV p24 antigen. Reprinted from Ref. [34] with permission from Lippincott Williams & Wilkins, Inc.

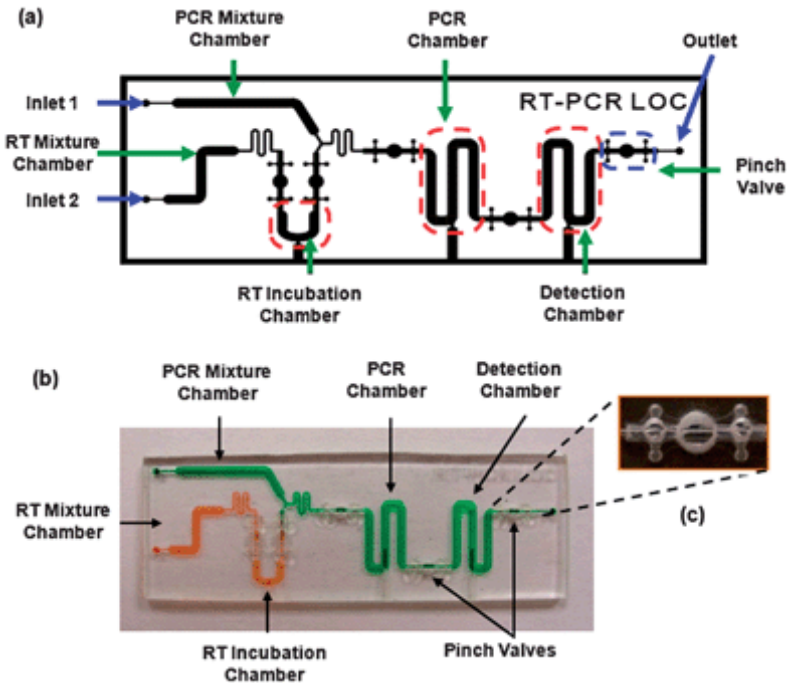

Fig. 4. Polymer-based device for on-chip PCR. Reproduced from Ref. [52] with permission from The Royal Society of Chemistry.

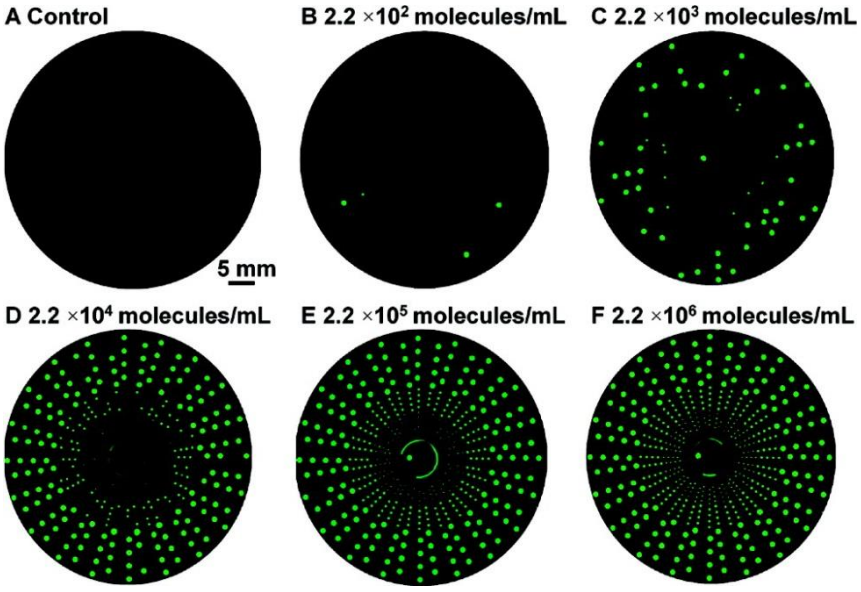

Fig. 5. Digital RT-PCR results on a rotational SlipChip. Reprinted with permission from Ref. [53] Copyright 2011 American Chemical Society.

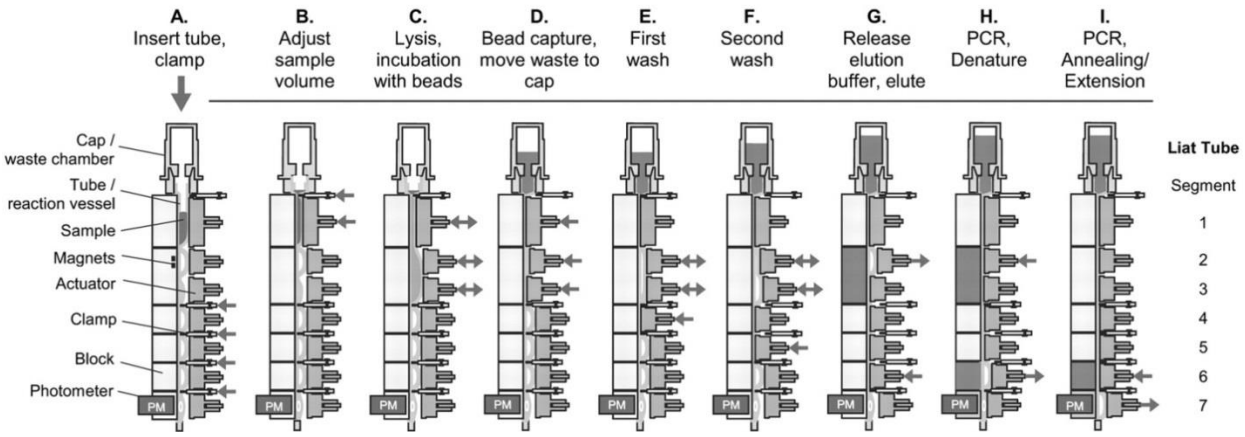

Fig. 6. Overview of Liat analyzer. Reprinted from Ref. [55] with permission from Oxford University Press.

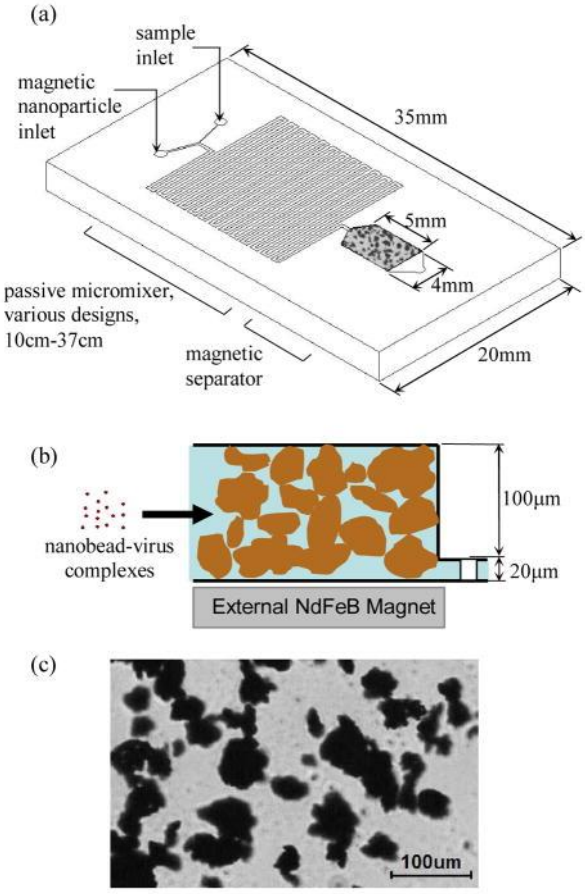

Fig. 7. Superparamagnetic nanoparticle capture device. Reprinted with permission from Ref. [59]. Copyright 2009 American Chemical Society.

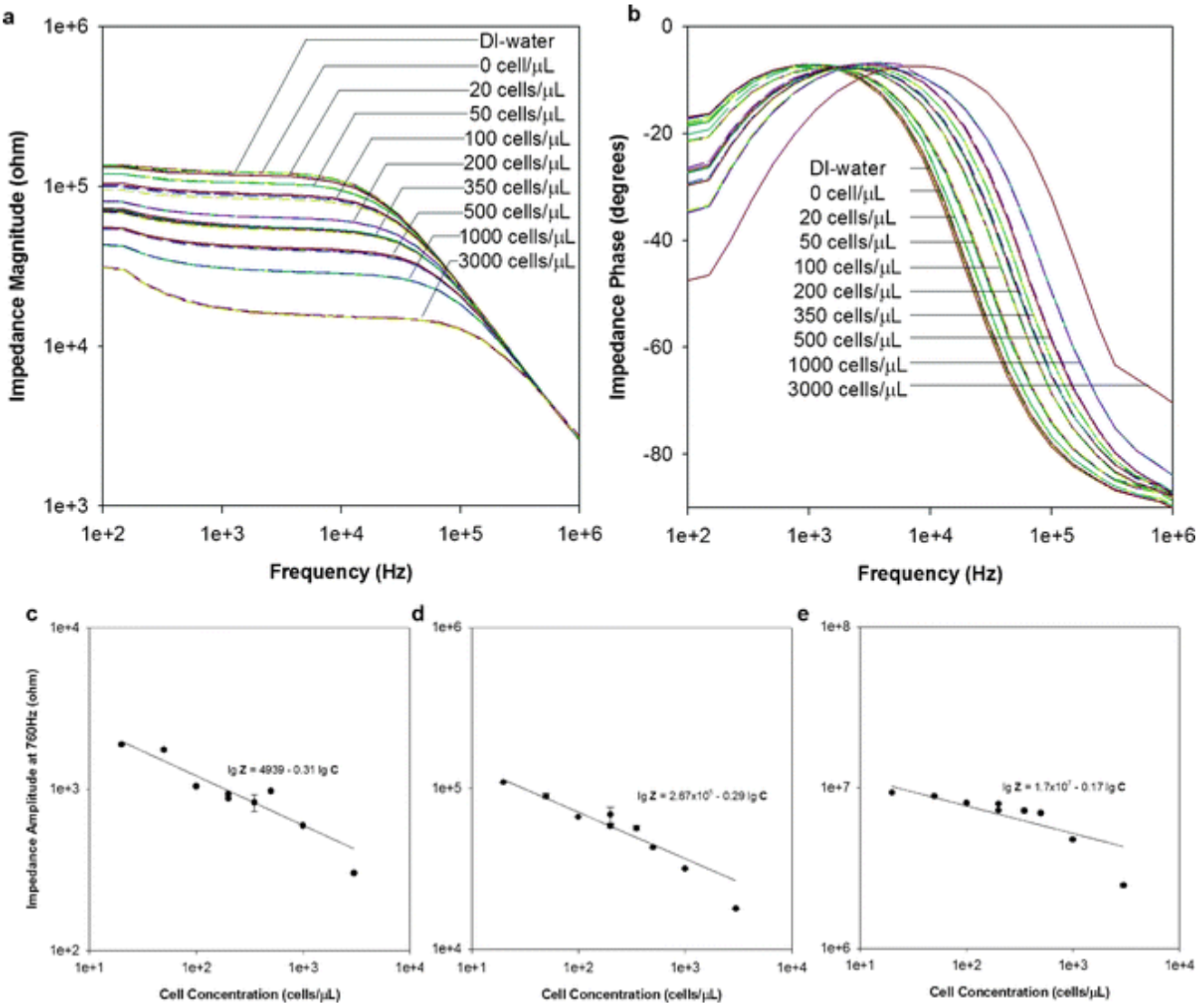

Fig. 8. Cell lysate impedance spectroscopy for enumeration of CD4 T lymphocytes. Reprinted from Ref. [109] with permission from The Royal Society of Chemistry.

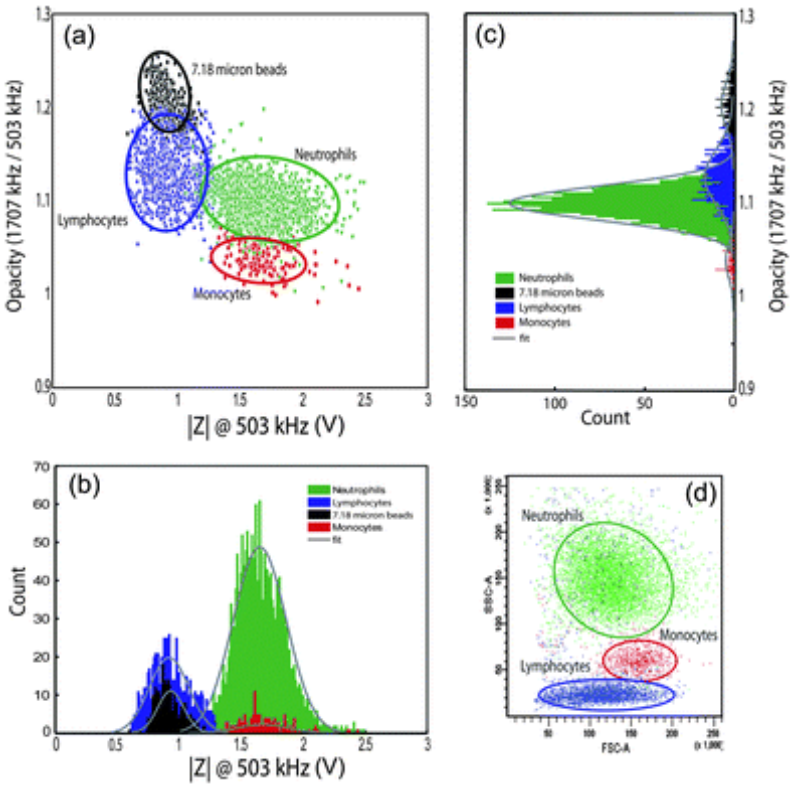

Fig. 9. Leukocyte type differentiation by dual-frequency impedance characteristics. Reprinted from Ref. [117] with permission from The Royal Society of Chemistry.

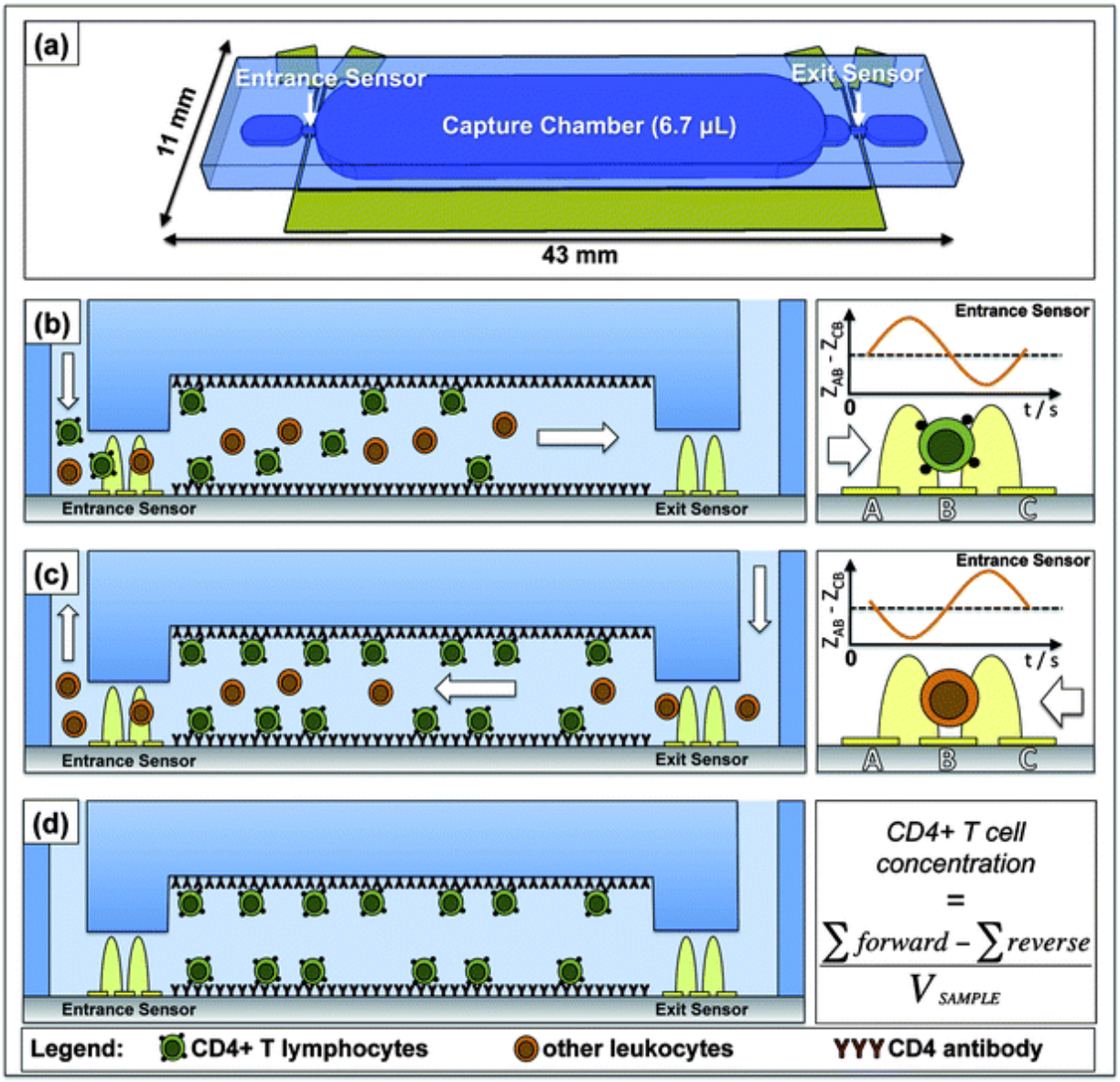

Fig. 10. Differential counter technique for CD4+ T cell enumeration. Reprinted from Ref. [121] with permission from The Royal Society of Chemistry.

3. Materials and Methods

The point-of-care detection of biological entities will play an essential role in the changing face of health care delivery by making the detection of disease and monitoring of treatment more ubiquitous in developed nations and more accessible in developing nations. Sensing platforms for biomolecular entities such as cardiac enzymes, cancer biomarkers, toxins, bacteria and viruses can dramatically improve clinical outcomes by enabling earlier diagnosis and personalized monitoring. In particular, populations residing in remote and resource-limited settings stand to benefit significantly from low-cost portable technologies capable of detecting the mediators of major communicable diseases.

As an example, 34 million people worldwide are living with human immunodeficiency virus (HIV), the virus that causes acquired immune deficiency syndrome (AIDS) and led to 1.8 million deaths in 2010 alone [1]. Among the greatest challenges in fighting HIV/AIDS globally is access to adequate healthcare in the world's poorest regions which are disproportionately affected by the epidemic [1]. This includes access to antiretroviral therapy as well as the diagnostic technologies required to inform administration of that therapy. The gold standards, flow cytometry for CD4+ T lymphocyte counting and nucleic acid amplification (PCR, NASBA, or bDNA assays) for determination of plasma viral load, require expensive instrumentation, skilled technicians, and lack the portability necessary to be employed in in remote and resource-limited settings. Furthermore, while it has been shown that early administration of therapy is critical to outcome [128], diagnosis of HIV status in adults is limited by the 2-8 week window period during which standard serological assays can produce false negatives [67]. A more accessible test for detecting HIV more immediately after infection could make great strides in combating the disease.

A critical need therefore remains for a low-cost HIV detection assay for the point-of-care which could provide (i) a qualitative assessment of plasma viremia, especially during the early weeks of infection prior to seroconversion, and (ii) a quantitative assessment of plasma viral load as a tool for informing treatment strategies in individuals with established HIV-positive status, especially during initial viremia when antibodies are undetectable but plasma viral load is in the range of 10^6 copies/ml [129].

Several micro- and nanotechnology solutions have been described in attempts toward point-of-care platforms for HIV/AIDS diagnostic applications [130]. These approaches have often included assays for the p24 viral capsid protein [32–36] and viral enzyme reverse transcriptase activity [38]. Others have attempted isothermal amplification of viral nucleic acid on point-of-care platforms [50], [51] or miniaturized polymerase chain reaction (PCR) [52], [53], [55]. Few approaches have attempted detection of whole virus particles for a point-of-care measurement, although strategies for the separation of HIV from whole blood or plasma for diagnostic assays by microfluidic immunoaffinity chromatography [56–58] and superparamagnetic nanoparticles [59] have been reported and may lend themselves well to a

whole particle detection approach. Many of the approaches reported to date, however, are not fully portable and automated, rely on expensive detection instrumentation, or do not demonstrate the sensitivity necessary to rival state-of-the-art nucleic acid amplification assays, thus a ubiquitous platform for point-of-care HIV viral load detection is yet to emerge.

The concept of lysate impedance spectroscopy was introduced by Cheng, et al. for the detection of human CD4+ T lymphocytes [109]. Cells were captured in a microfluidic channel and lysed by the addition of low-conductivity hypotonic solution and impedance changes detected by surface electrodes were showed to be indicative of cell number down to just 20 cells μl^{-1}. Others have applied impedance spectroscopy more broadly for the detection of bacterial growth, [131], [132] binding of an analyte to a recognition site on electrodes [133], and, recently, the qualitative detection of HIV from viral lysis at high concentrations [134].

The concept of releasing liposome contents as a biosensor component has been reported in the past; however, the materials encapsulated by the liposomes in these cases were either fluorescent molecules or redox couples [135–141]. Our ion-encapsulating liposomes represent a simpler approach which would better accommodate the requirements for portable sensing platforms.

Here we report an ELISA-inspired approach to biological detection consisting entirely of on-chip electrical impedance sensing and apply to HIV detection. At the core of this detection strategy is a micron-sized, antibody-functionalized liposome particle encapsulating concentrated phosphate buffered saline (PBS). These liposome tags can be quantified by impedance spectroscopy upon ion release in low conductivity media and are also shown to specifically bind surface-immobilized virus particles captured in a microfluidic channel. Here we characterize dipalmitoylphosphatidylcholine (DPPC) liposome particles, show quantification by this electrical sensing method, and demonstrate an ELISA-like approach to virus capture, liposome tagging and sensing.

3.1 Modelling of impedance spectroscopy

3.1.1 Conductivity changes from liposome ion release

The change in impedance sensed by our system is the result of ion release into the surrounding media from the permeabilization of liposomes. The average diameter of liposomes used in this report (see Fig. 11) was determined to be 3.7 μm, which corresponds to an average volume of 26.5 fL per liposome. Each liposome encapsulated 10X PBS containing 1.37 M NaCl and 0.027 M KCl. Each liposome therefore contributes approximately 3.6 × 10-14 moles of NaCl to the surrounding media upon complete release of its contents. Assuming that the beginning solution is true deionized water (conductivity of 0.055 MΩ-1 cm^{-1}) [142], 33,000 liposomes (~5,000 liposomes per μl) would produce a 0.18 mM change in NaCl in the 6.628 μl volume fluidic channel. Assuming the effects on conductivity of NaCl in 10X PBS dominates over the effects of KCl, this change in ion concentration can be calculated to produce a change per

liposome per microliter of approximately 4.27 $G\Omega^{-1}$ cm^{-1} [142], [143]. It has been shown previously that change in capacitance from ion release into solution is several orders of magnitude lower than the change in bulk conductance, thus the effect on conductance dominates [109].

3.1.2 Modelling impedance spectra

Electrodes in solution can be modelled by the equivalent circuit in Fig. 14d. In this simplified model, C_{di} is the dielectric capacitance resulting from all materials surrounding the electrodes, R_{sol} is the solution resistance, R_{ser} is the series resistance of the electrodes and wires, and Z_{para} is the parasitic impedance, which is measured from the open circuit [109], [131], [132]. Z_{dl}, the interfacial or Warburg resistance, is described by

$$Z_{dl} = [(j\omega)nB]^{-1} \quad (1)$$

Where $j = \sqrt{(-1)}$, and the parameters n and B depend on the properties of the electrolytes and electrodes [109], [131], [132]. This model will be used to fit the impedance spectra of liposome ion release in the interdigitated electrode device described here.

3.2 Reagents

1,2-dipalmitoyl-sn-glycero-3-phosphocholine (DPPC) and 1-palmitoyl-2-{12-[(7-nitro-2-1,3-benzoxadiazol-4-yl)amino]dodecanoyl}-sn-glycero-3-phosphocholine (NBD PC) were purchased from Avanti Polar Lipids (Alabaster, AL, USA). Protein A was purchased from ProSpec (East Brunswick, NJ, USA). Phosphate buffered saline (10X solution) was purchased from Fisher Scientific (Hampton, NH, USA) and Lonza (Basel, Switzerland). Sucrose, dextrose and Triton X-100, deoxycholic acid, sodium azide palmitic acid N-hydroxysuccinimide (pal-NHS), and rhodamine B isothiocyanate were purchased from Sigma-Aldrich (St. Louis, MO, USA). Calcein was purchased from Fisher Scientific (Hampton, NH, USA). Anit-gp120 goat IgG was purchased from Abcam (Cambridge, MA, USA). Virus buffer consisted of Tris, NaCl, and EDTA purchased from Sigma-Aldrich (St. Louis, MO, USA). HIV-1 strain IIIB was purchased from Advanced Biotechnologies Inc. (Columbia, MD, USA).

3.3 Preparation of liposomes

DPPC was dissolved in chloroform and dried in a round bottom flask by rotary evaporation. The lipid film was hydrated with 10X PBS at 50 degrees C to create liposomes at a lipid concentration of 1 mg/ml. This mixture was then sonicated for 15 minutes in an ice bath.

To create fluorescent NBD-liposomes, NBD-PC lipids were dissolved with DPPC at 1 mol%. Liposomes were then formed by the same hydration and sonication processes described above.

3.4 Devices

Planar interdigitated electrode chips were fabricated on glass with standard photolithography and gold lift-off technique. A polydimethylsiloxane (PDMS) cover 4 mm x 34 mm x 50 μm (6.628 μl total volume)

was cured on a master mold of SU-8 photoresist patterned on a 4" silicon wafer using standard photolithography technique. Inlet and outlet ports were punched in each PDMS cover, which were then aligned with the electrodes and bonded after oxygen plasma activation in a barrel etcher. A schematic and photograph of the device are provided in Fig. 11.

3.5 Liposome stability characterization

NBD-liposomes were prepared in 10X PBS as described above. Initially, four samples were each added to deionized (DI) water, centrifuged at 3220 rcf for 10 minutes to pellet the liposomes, and the supernatant was aspirated. The pellet was then re-suspended in DI water and the process was repeated to achieve thorough washing. After the second aspiration of supernatant, each pellet was re-suspended in 10X PBS, 1X PBS, sugar solution, or DI water. Each sample was well-mixed by pipetting up and down to ensure even re-suspension of the pellet and placed on a sample rotisserie to prevent settling. Liposome number was assessed regularly for each sample by a Guava EasyCyt Plus flow cytometer (EMD Millipore, Billerica, MA, USA) over the course of several hours.

To consider the effects of detergent on liposome stability, NBD-liposomes were washed as described above and re-suspended in DI water or DI water containing 1% v/v Triton X-100. Samples were placed on a sample rotisserie and analysed by flow cytometry over the course of several hours.

To consider the effects of heating on similar samples, NBD-liposomes were washed and re-suspended in DI water or 1% v/v Triton X. Each sample was aliquoted into several vials which were independently heated to temperatures ranging from 30 degrees C to 99 degrees C. After heating and cooling to room temperature, liposomes were analysed in a flow cytometer to determine liposome number.

3.6 Liposome permeability characterization

Liposomes were prepared in 10X PBS containing 50 mM calcein and washed twice by adding an equal volume of DI water, centrifugation and aspiration of supernatant. After the second wash, liposomes were re-suspended in 10X PBS, 1X PBS, sugar solution, or DI water and added as eight replicates of each sample in 0.2 ml PCR reaction tubes. This reaction strip was placed in a Mastercycler ep realplex real time PCR system (Eppendorf, Hauppauge, NY, USA) for temperature analysis. The sample temperature was increased from 25 degrees C to 95 degrees C over 30 minutes and at 520 nm emission was monitored throughout. Control samples containing 10X PBS without calcein were also analysed in the same assay.

3.7 Heat-induced liposome permeabilization for impedance spectroscopy

NBD-liposomes were washed and re-suspended in DI water in four different concentrations. Serial dilutions of each of these liposome suspensions were performed in DI water to achieve the desired range of liposome number. A dilution within the range of the flow cytometer was analysed to determine liposome concentration for each of the four sample sets. Samples were heated to 50 degrees C for 15

minutes and allowed to cool to room temperature. Each sample was then injected into the interdigitated electrode chip for impedance spectroscopy analysis.

3.8 Impedance spectroscopy measurements

Impedance magnitude and phase angle were determined using an Agilent 4284 LCR meter (Agilent Technologies Inc., Palo Alto, CA, USA). Micromanipulator probes were used to connect the microfabricated device to the LCR meter and the measurement process was automated by MATLAB (MathWorks, Natick, MA, USA). Impedance spectra were measured for frequencies between 100 Hz and 1 MHz with an increase factor of 1.5 and amplitude of 250 mV.

3.9 Real-time impedance monitoring of ion release from liposomes

NBD-liposomes were prepared and washed as described previously. However, to ensure complete elimination of ionic contamination from liposome samples, each wash was performed in a 50 ml centrifuge tube and repeated twice for a total of three washes. Liposomes were then suspended at various solutions and a portion of the sample was immediately analysed by flow cytometry to determine liposome number. Within one minute of re-suspension in DI water, the liposome sample was injected into the interdigitated electrode device. The device was set on a heating stage and held at 23 degrees C for 30 seconds before being heated to 50 degrees C and held for several minutes. Impedance was monitored throughout at 2 kHz and 10 kHz.

3.10 Preparation of antibody-functionalized liposomes

Protein A was hydrophobically modified with hexadecyl chains for anchoring on the liposome surface. Briefly, 1mg of protein A was reacted with 0.1 mg of pal-NHS in a solution of 0.3% deoxycholic acid and 0.1% sodium azide in 1X PBS according to the procedure described by Kim and Peacock [144]. After reacting for 24 hours at room temperature, palmitated protein A was purified by centrifuge filter (MWCO 3kDa, Millipore).

Protein A was adsorbed to liposomes by mixing 5 μg of palmitate-modified protein A for every 1 mg of lipid. The mixture was incubated for 12 hours at room temperature, followed by addition of DI water to pellet the liposomes upon centrifugation for 10 minutes at 3220 rcf to remove protein A that was not adsorbed.

To verify adsorption of protein A, the protein was fluorescently labeled with the amine-reactive rhodamine B isothiocyanate, followed by purification by centrifugal filtration and dialysis to remove unreacted rhodamine. This fluorescent palmitated protein A was incubated with liposomes, which were then purified by centrifugation as described. Fluorescent intensity of the supernatant and re-suspended liposomes was recorded with a Tecan Infinite 200 PRO (Tecan AG, Switzerland), indicating that 40% of the protein A initially added remained adsorbed to the liposomes.

Liposomes with protein A were then mixed with 18 μg/ml anti-gp120 IgG for four hours on a sample rotisserie.

3.11 Virus detection by heat-induced liposome permeabilization

Interdigitated electrode devices were infused with 25 μl of 0.3 mg/ml anti-gp120 IgG in PBS and incubated at 4 degrees C overnight. Excess antibody was rinsed from the fluidic chamber with 100 μl PBS flowing at 10 μl min^{-1}. Following this rinse, 50 μl buffer containing 6.7e11 virus particles per μl or buffer without viruses was infused into each device at 5 μl min^{-1} and incubated for approximately four hours. Following incubation, each device was rinsed with 100 μl PBS at 10 μl min^{-1} to remove the buffer and unbound viruses. Subsequently, 100 μl of 6,537±70 μl^{-1} liposomes functionalized with anti-gp120 IgG were injected at a rate of 10 μl min^{-1} followed immediately by rinsing with 200 μl DI water at 20 μl min^{-1} to rinse away unbound liposomes and lower the conductivity of the bulk solution. Each device was then placed on a heating stage and real-time impedance was measured during heating as described above.

Figures

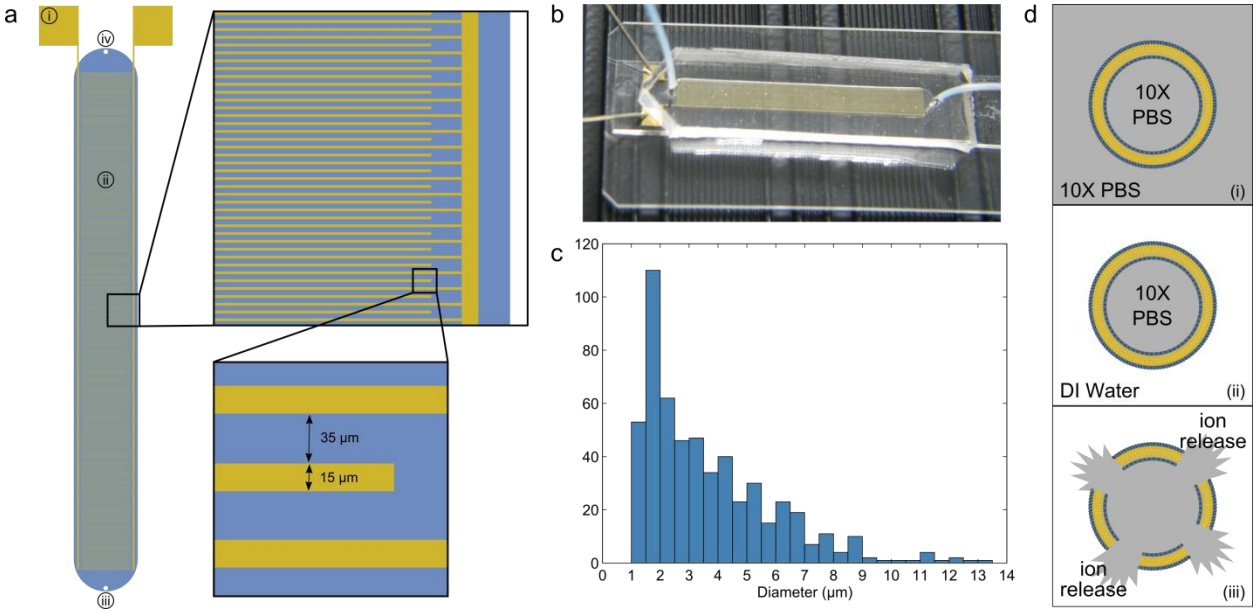

Fig. 11 (a) Schematic of interdigitated electrode impedance sensing device. Each electrode finger is 15 µm wide with a 35 µm gap between electrodes. Labeled components are (i) gold contact pads where micromanipulator probes contact the device, (ii) sensing region/fluidic chamber, (iii) fluidic inlet port, (iv) fluidic outlet port. The blue region represents the fluidic chamber defined by the PDMS cover. (b) Photograph of device with PDMS cover mounted on a microscope slide. Micromanipulator probes can be seen in contact with the device. (c) Histogram of liposome diameters as determined by optical microscopy (mean diameter = 3.682 µm, standard deviation = 2.262 µm) and analysis with ImageJ software. (d) Illustration of liposome sensing concept: (i) liposomes are hydrated in 10X PBS, producing ion-encapsulating particles, (ii) the external media is replaced with low-conductivity DI water, (iii) ion release is triggered and impedance change is measured in order to quantify liposomes present in the sensing device.

4. Results and Discussion

4.1 Liposome stability characterization

To determine the stability of liposomes in various media, flow cytometry measurements were recorded over several hours with NBD-liposomes. Three replicates each of liposomes suspended in isotonic (10X PBS) and hypotonic (1X PBS, sugar solution, DI water) media were measured to assess the effects of various osmotic forces. Sugar solution was chosen because it has been used in the past as an approach to maintaining lymphocyte stability when a low-conductivity medium is desired for impedance measurements of cell lysate [109]. The 8.5% sucrose/0.3% dextrose solution used in these measurements would have approximately the same osmolarity as cytosol or 1X PBS. A sugar solution which matches the osmolarity of 10X PBS is not practical (too viscous) and therefore was not investigated.

Flow cytometry analysis of liposomes in the four media considered showed little to no decrease in both PBS samples and some depletion in both sugar and DI water over approximately fourteen hours. To analyse the counting data for each sample, each replicate was fitted separately and the three fits were averaged. This averaged fit is presented in Fig. 12a. The slope of the fits showed depletion rates of approximately 0.0905% min^{-1}, 0.0569% min^{-1}, 0.0089% min^{-1}, and 0.0125% min^{-1} for DI water, sugar solution, 1X PBS and 10X PBS respectively (Fig. 12a, inset).

In order to compare the stability of liposomes in DI water with a common liposome permeabilization/lysis reagent, Triton X-100, a separate flow-cytometry measurement was performed with liposomes in DI water and 1% Triton X. In this case, liposomes with and without membrane-integrated protein A were also compared to determine if liposome functionalization would compromise stability. The results, presented in Fig. 12b, show that liposomes are compromised in the presence of detergent, showing rapid depletion in the first hour and nearly 100% depletion of liposomes after five hours. The presence of adsorbed protein A showed little effect.

Upon initial consideration of heating as a chemical-free permeabilization technique for liposome impedance sensing, liposomes in DI water and 1% Triton X were also analysed by flow cytometry after heating to various temperatures. Counting data in Fig. 12c shows that the destabilizing effects on the liposomes of detergent were accelerated by the addition of heat to the solution. A proposed mechanism explaining the behavior of liposomes upon heating and in the presence of detergent is provided in the Discussion section of this paper.

4.2 Effects of heat on liposome stability

A DNA melting curve assay proved to be the ideal measurement for characterizing the effects of heating on liposome stability and to determine the critical temperature, which we define as the temperature at which the lipid bilayer is partially compromised and encapsulated contents are released

into the surrounding media. An ideal reporter molecule for this measurement was calcein, a fluorescent dye which self-quenches at millimolar concentrations [145], [146].

Liposomes were prepared in concentrated calcein and removed from free calcein in surrounding media by centrifugation and re-suspension of the liposome pellet. Calcein encapsulated within liposomes exhibited very little emission at 520 nm. Upon heating in the thermocycler, however, a sharp increase in fluorescence is observed in the range of 40-43 degrees C, indicating the release of liposome contents as calcein dissociates and self-quenching subsides. A plot of raw fluorescence is presented in Fig. 13a, with the first derivative with respect to temperature, dI/dT, presented in Fig. 13b as reported by the instrument's data analysis software.

4.3 Liposome quantification by ion-release impedance spectroscopy

The quantification of liposomes by impedance spectroscopy was demonstrated by suspension of liposomes at various concentrations in DI water and off-chip heating to promote release of encapsulated ions. After cooling to room temperature, each sample was injected into the fluidic chamber and impedance spectra were measured. The measured impedance depends on the concentration of ions in the fluid. We assume the average liposome size is consistent between measurements and that all liposomes encapsulate 10X PBS, which allows for impedance to be directly related to liposome number. Figs. 14a-b show the impedance magnitude and phase angle versus AC frequency for each sample. In Fig. 14c, the impedance recorded at 2.6 kHz is plotted versus liposome concentration as measured by a flow cytometer. A lower limit of detection was determined to be at a liposome concentration of approximately 103 μl^{-1} and impedance values measured at concentrations above this were fitted with a straight line on log-log axes.

4.4 Impedance modelling

The simplified circuit model in Fig. 14d was used to fit measurements displayed in Figs. 14a-b. The parasitic impedance Zpara was determined by fitting the impedance data measured with the device prior to adding any fluid and was then held constant for the other fits. Examples of fits with the measured data are provided in Figs. 14e-f. The bulk conductance $G_{sol} = 1/R_{sol}$ can be determined from the parameters extracted for each measurement and are plotted in Fig. 14g versus liposome concentration [109]. The slope of the fit to conductivity data gives the sensitivity of the interdigitated electrode chip, determined in this case to be 16.022 $G\Omega^{-1}$ (liposomes per $\mu l)^{-1}$ [109].

4.5 Real-time impedance monitoring and quantification

Ion release from liposomes was monitored in real time and the resulting impedance trace could be used to determine liposome concentration as described above. 10X PBS-containing liposomes in DI water were injected into the interdigitated electrode device which was placed on a small heating stage. The

temperature was held constant near room temperature for 30 seconds and quickly increased to 50 degrees C where it was held constant until the measurement completed. Because conductivity increases with temperature, the impedance trace shows an initial steady decrease as a result of heating of the device; however, a second, sharper decrease is observed as the device reaches critical temperature and the encapsulated ions are released. Sample traces of this behavior are presented as the normalized impedance over time in Fig. 15a and the time derivative of normalized impedance in Fig. 15c. Figs. 15b and 15d show two methods for quantifying liposomes from this data: by fitting the normalized impedance after 200 seconds (Fig. 15b) and by determining the maximum rate of change (Fig. 15d). Once again, the signals produced by samples below concentrations of 10^3 ml^{-1} appear commensurate with measurements of DI water and are not included in fitting of the data.

4.6 Virus detection

As a proof-of-concept toward liposome ion-release impedance spectroscopy for virus detection, several devices were functionalized with anti-gp120 antibody and exposed to 6.7e11 μl^{-1} HIV to be compared with controls. After prolonged exposure to the virus, the devices were rinsed and 100 µl of IgG-functionalized liposomes (6,537±70 μl^{-1}) in PBS were injected through the device, followed immediately by rinsing with 200 µl DI water. A schematic of this ELISA-like assay is depicted in Fig. 16a. The same heating and real-time impedance monitoring protocols as described above were followed for analysis of these devices, and the normalized impedance after 200 seconds for devices prepared with immobilized viruses is compared with a control treated with virus-free buffer. Fig. 16b shows the normalized impedance data and Fig. 16c summarizes data from four separate devices for each case, showing a significantly larger change in impedance after 200 seconds for virus-containing devices, representing specific capture of liposomes on immobilized HIV.

4.7 Discussion

This paper describes progress toward an ELISA-like liposome-based impedance sensing device for biological sensing at the point-of-care. We begin with the characterization of liposome particles containing 10X PBS which are the basis for electrical sensing, providing a simple and low-cost solution to detection of submicron particles. Liposome stability over time is compared in four different media, demonstrating that although liposome depletion rate is greatest in DI water as the result of osmotic forces, the loss of particles is still minimal over a short time span. In our assay, the exposure of liposomes to pure DI water is anticipated to be 10 minutes or less, thus this minimal depletion rate is inconsequential. This is a marked difference from the effects of DI water on human T lymphocytes where it was used by Cheng, et al. to promote rapid lysis of human cells [109].

Liposome stability in DI water was also compared to stability in the presence of the detergent Triton X, a reagent which is used ubiquitously to restructure lipid membranes. We believe that the detergent

disrupts the liposomes by inserting itself into the lipid bilayers, thus increasing permeability. At a constant temperature, rupture of the entire liposome population appears to occur over several hours and appears to be accelerated by heating the sample.

While heating characterization described in Fig. 13 demonstrates that liposomes release encapsulated materials above a temperature of approximately 41 degrees, consistent with the lipid phase transition temperature of DPPC, the counting of liposomes in DI water as shown in Fig. 12c indicates that even upon heating the sample near boiling point (99 degrees C), the liposome population is not significantly decreased upon cooling and counting in the flow cytometer. This phenomenon can likely be explained by the self-repair properties of the lipids. Above the transition temperature, the kinetic energy of these molecules is enough to overcome the hydrophobic interactions which stabilize the bilayer structure, thus explaining the release of encapsulated ions. Flow cytometry analysis, however, is performed after the sample has been cooled again. The data in Fig. 12c is explained by the presence or absence of detergent – without Triton X, DPPC lipids are free to re-stabilize their ordered bilayer structures, while reformation of liposomes is inhibited by Triton X, which favours the formation of micelles and may sequester or destabilize DPPC lipids.

In the quantification of human T lymphocytes by lysate impedance spectroscopy [109], the introduction of DI water is used to trigger lysis of cells and release of contents for interrogation. In this measurement, liposomes are more stable in DI water, likely as a result of the absence of membrane proteins, particularly aquaporins, which would allow for the diffusion of water molecules into the cell driven by the osmostic gradient.

DI water is therefore not a suitable technique for triggering liposome permeabilization. Furthermore, chemical-based permeabilization is not preferred for this platform because the introduction of a reagent by flow necessarily results in the displacement of an equal volume of fluid from the microfluidic chamber and thus may result in the loss of lipids or ions and complication of the impedance measurement. Heating is therefore an ideal technique for stimulating the release of encapsulated ions from liposomes in the fluidic chamber as it allows for interrogation of the chamber without displacing its contents.

Liposomes were initially prepared containing 1X PBS, however, 10X PBS was later employed as a means of amplifying the signal produced by liposome permeabilization and is used in all the data presented here. The lower limit of detection determined by the data in Fig. 14 shows the same signal as the deionized water we obtained for our experiments. It is evident that the DI water that was available to us did contain some small amount of ionic contamination and we anticipate that a higher sensitivity would be possible if DI water containing fewer ions were available. We believe that this was the case for the similar measurements performed with human T lymphocytes in [109] where a lower limit of detection is demonstrated.

We have demonstrated that the sensing device used in these measurements can be modeled with a simple circuit consisting of a capacitor, C_{di}, in parallel with parasitic impedance Z_{para} and the series combination of solution resistance R_{sol} and interfacial impedance Z_{dl}. From this model, the value R_{sol} is used to determine the bulk solution conductance, G_{sol}, which is related to the solution conductivity σ by the equation:

$$G = \sigma mA/L \tag{2}$$

Where A is the solution cross-sectional areas between electrodes, L is the spacing between electrodes, and m is the number of electrodes [109]. For our device, the value of mA/L is 133.7 cm and this value can be used to determine a measured conductivity change of 0.12 $G\Omega^{-1}$ cm^{-1} (liposomes per μl)$^{-1}$. This differs by one order of magnitude from our predicted conductivity change of 4.27 $G\Omega^{-1}$ cm^{-1} (liposomes per μl)$^{-1}$, but can be attributed to the behaviour of ions in bulk as described by Chen, et al. [109].

During real-time monitoring of liposome permeabilization, two methods for quantification are demonstrated (Fig. 15): normalized impedance after 200 seconds and max –dZ/dt. It is still to be determined which method is a more consistent and sensitive method for detection. An improved technique which minimizes the fluctuation of device temperature during heating and heats the device more slowly may result in a lower baseline in the time derivative and thus allow for a lower limit of detection. This technique is to be optimized in future studies.

Additionally, the liposomes described in this report exhibited significant variation in diameter. We anticipate that the decrease in impedance magnitude and –dZ/dt would correlate better if liposome size was uniform. Several microfluidic techniques which produce highly uniform liposome particles have been described [147], [148]. These formation methods can be pursued in future work for a more accurate liposome-based measurement.

The accuracy and sensitivity of this device may also be improved by employing larger liposomes. We found that the lower limit of detection was approximately 1,000 liposomes/μl in our current measurements (average liposome diameter = 3.7 μm). Because the impedance change detected depends on the total volume of 10X PBS released from all liposomes on the device, larger liposomes would enable the sensing of fewer total particles. Furthermore, because the volume of a sphere scales with the radius cubed, a liposome with twice the radius of those used in our measurements would have eight times the volume. In other words, only one eighth of the number of liposomes per microliter would be needed to produce the same impedance change and fewer liposomes per microliter could be detected. As an example, a 10 μm diameter liposome has 19.7 times the volume of a 3.7 μm diameter liposome. We

would expect, therefore, to be able to detect approximately 50 liposomes/μl if 10 μm liposomes were used.

Finally, the qualitative sensing of viruses based on impedance change that we demonstrated is only a proof-of-concept. The time of incubation with virus sample was prolonged in our current study to ensure ample time for virus immobilization. We believe, however, that efficient and rapid capture of viruses can be achieved with optimized device geometry, antibody immobilization methods, and improved protocols for virus capture. We are now pursuing the quantitative detection of viruses after high-efficiency immunocapture from whole blood or plasma from HIV-positive individuals.

Figures

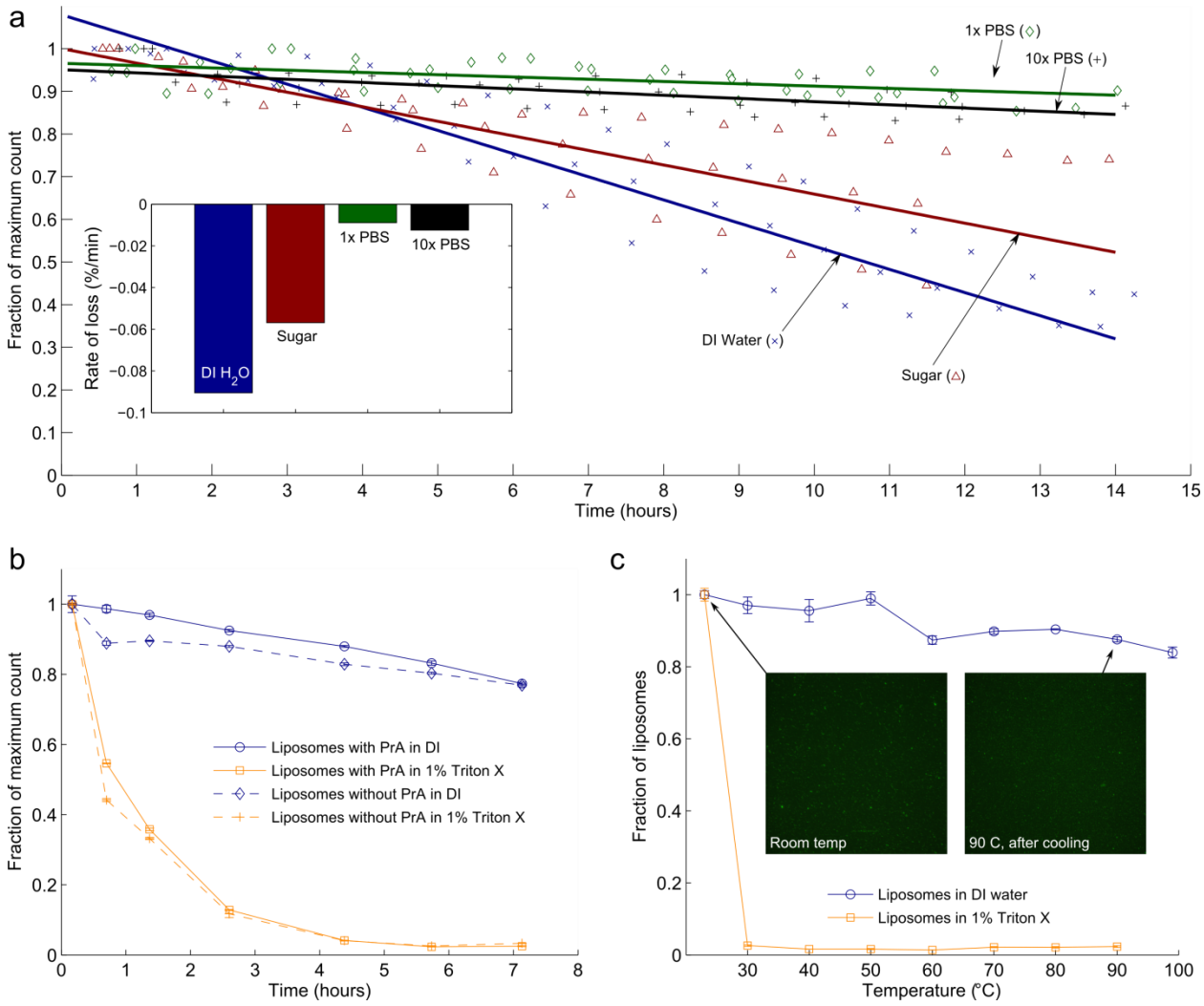

Fig. 12 Liposomes in various conditions were counted by flow cytometry to characterize stability. (a) Liposome count was measured over several hours in DI water, sugar solution, 1X PBS, and 10X PBS. The measurement was repeated for each condition for a total of three samples. Each repeat was fitted with a linear best fit. The average of the three fits is shown. (inset) Bar chart of slopes determined from averaged fits of three repeats of each condition. (b) Liposomes with and without protein A were suspended in DI water and 1% Triton X. Counting over time shows that detergent accelerates liposome depletion. (c) Similarly, liposomes were suspended in DI water and 1% Triton X, heated to various temperatures and counted with a flow cytometer after cooling to room temperature. This data suggests that heating accelerates the effects of detergent but does not compromise the overall structure of liposomes in DI, although additional data presented in this paper indicates that heating above ~41 degrees C promotes the release of liposome contents. Fluorescence microscopy images of samples at room temperature and after cooling from 90 degrees confirm flow cytometry measurements by demonstrating that liposome particles are still present after extreme heating.

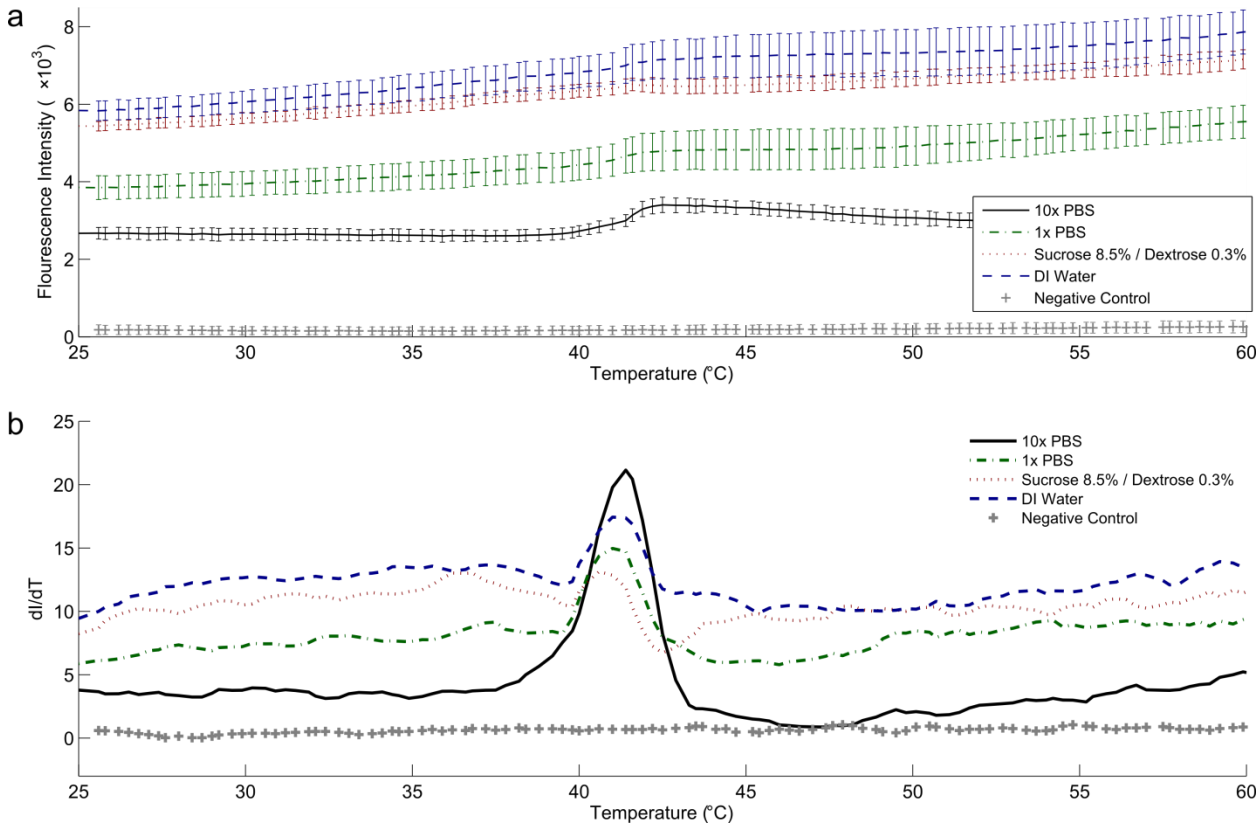

Fig. 13 Liposomes encapsulating calcein were prepared, re-suspended in various media and analyzed with a melting curve program in a realtime PCR instrument. The sample temperature was increased from 25 degrees C to 95 degrees C over 30 minutes and at 520 nm emission was monitored throughout. (a) Raw fluorescence intensity and (b) the rate of change dI/dT versus temperature show that a dramatic increase in fluorescence intensity occurs at approximately 41 degrees, indicating the release of calcein from within liposomes. This agrees with the lipid transition temperature cited by the product literature.

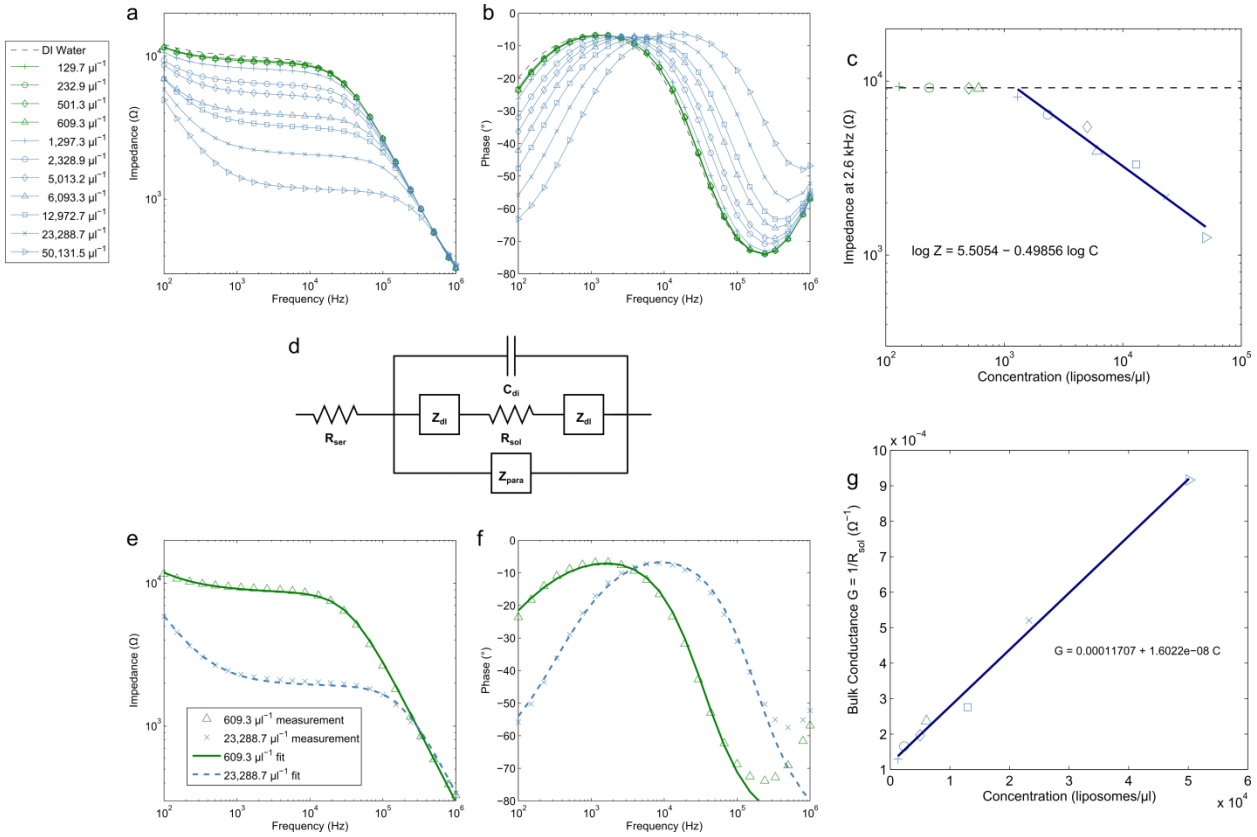

Fig. 14 (a-b) Ion-release impedance spectroscopy measurements from several heat-permeabilized liposome samples at concentrations ranging from 129.7 μl^{-1} to 50,131.5 μl^{-1} and (c) impedance measured at 2.6 kHz versus liposome concentration with fits to measurements above the limit of detection, approximately 1000 μl^{-1}. (d) Simplified circuit model of electrodes in solution which is fitted to experimental data, accounting for the dielectric capacitance C_{di}, solution resistance R_{sol}, series resistance R_{ser}, parasitic impedance Z_{para}, and interfacial impedance Z_{dl}. (e-f) Sample fits of the simplified circuit model to measured data for high and low concentrations. (g) Bulk conductance calculated from values for R_{sol} extracted from fitting the experimental data are plotted versus liposome concentration and fitted with a straight line. The slope of this line represents the sensitivity of the device.

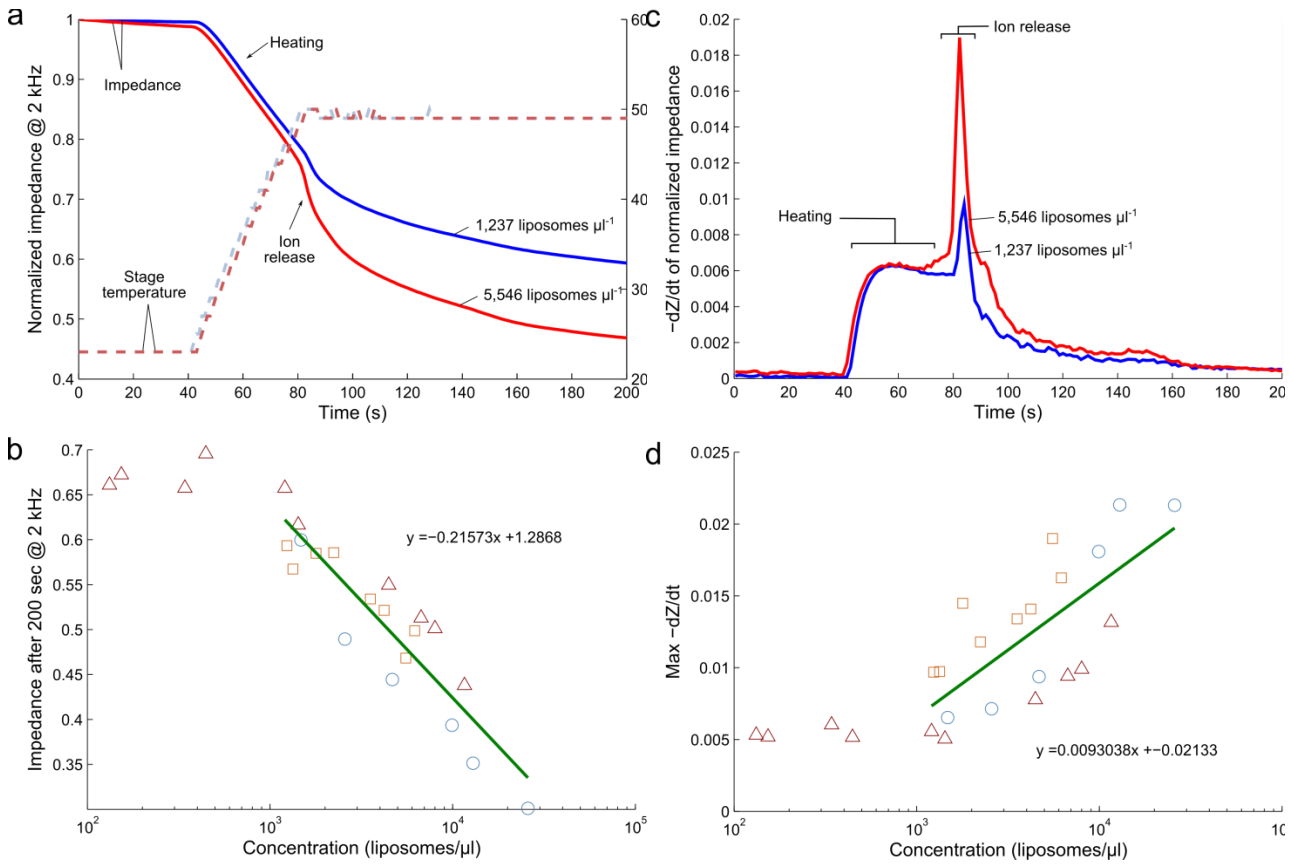

Fig. 15 Real-time impedance detection of ion release from liposomes by heating of interdigitated electrode device. (a) Sample data for liposomes at two different concentrations is shown, including the normalized impedance and the stage temperature for 1,237 μl^{-1} and 5,546 μl^{-1} samples. The actual device temperature lags behind the stage temperature by a few seconds because it is insulated by a glass microscope slide. (b) Shows the normalized impedance value at 200 seconds for all samples versus liposome concentration with linear best fit (on a semilog axis). Measurements indicated by each unique symbol/color combination were recorded from the same batch of liposomes. Three different batches of liposomes were prepared and measured in total. (c) The rate of normalized impedance decrease, –dZ/dt, is plotted for the same two representative samples. (d) Summarizes all measurements with the same symbol/color scheme and linear best fit (on a semilog axis). Only liposome concentrations above the lower limit of detection (10^3 μl^{-1}) are fitted.

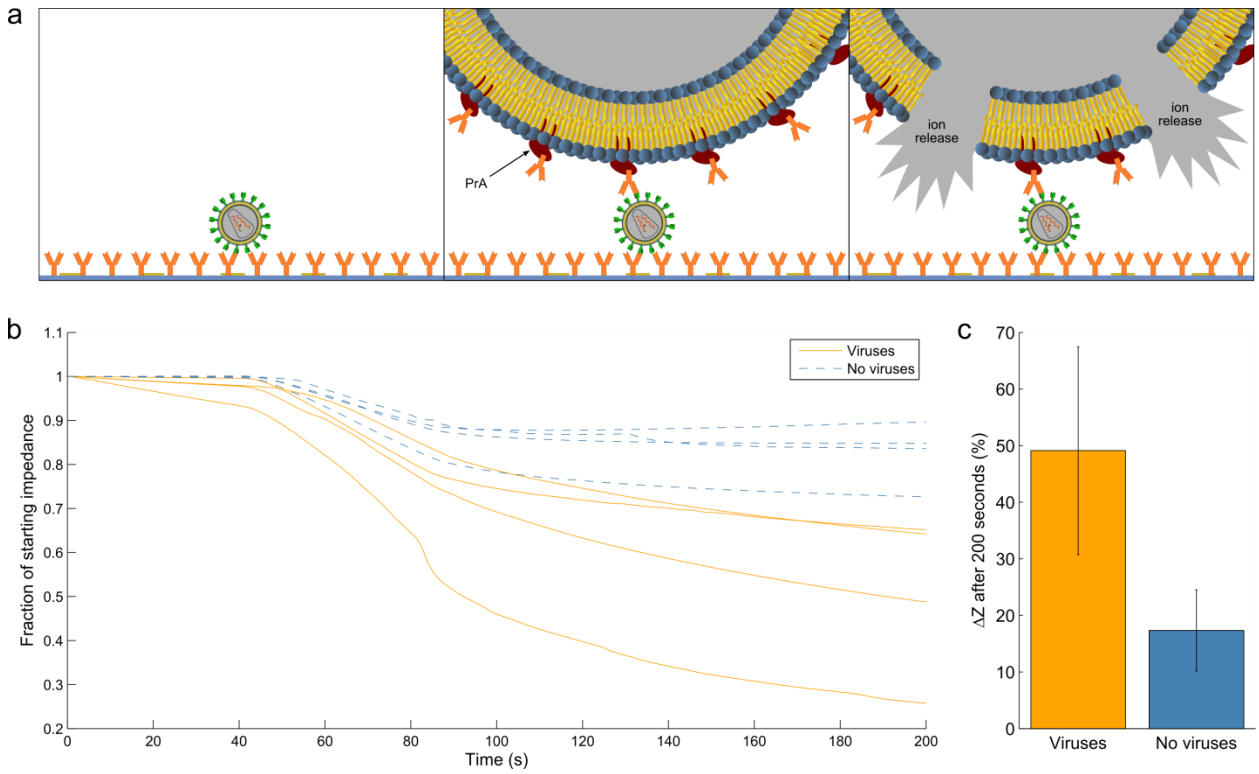

Fig. 16 Virus sensing by liposome tagging and ion-release impedance spectroscopy. (a) Concept of detection: (1) Virus is immobilized by antibody binding on the surface of the microfluidic channel. (2) Liposomes, functionalized with protein A (PrA) which binds the Fc region of IgG, bind specifically to immobilized viruses and background media is replaced by DI water. (3) Device is heated to trigger the release of encapsulated ions. (b) Normalized impedance data measured at 2 kHz for four repeats of virus-containing devices and controls. (c) Summary of average impedance change after 200 seconds for virus-containing devices (mean = 49.11%, standard deviation = 18.37%, n = 4) versus control (mean = 17.34%, standard deviation = 7.18%, n = 4). The averages are confirmed by two-tailed t-test to be significantly different with 95% confidence (t = 3.22).

5. Conclusion

We have shown the sensing of viruses by tagging with functionalized ion-encapsulating liposomes and detection with ion-release impedance spectroscopy. This approach to biosensing seeks to address fundamental barriers which render current state-of-the-art diagnostic instrumentation inaccessible in many remote and resource-limited parts of the world. We address this primarily through the integration of an entirely electrically-based sensing technology with simple components. This antigen-recognition based biosensor assay also contains an inherent a high degree of flexibility that could be accomplished by simply changing the antibody used.

This ion-release impedance sensor is an ongoing project and next steps will include strides toward a fully-integrated whole blood analysis platform for quantitative detection of HIV plasma viral load. Specifically, these steps include:

- Characterization of immunoaffinity capture of viruses from whole blood in a microfluidic device. The device will be functionalized with anti-gp120 IgG and HIV-negative blood specimens will be spiked with viruses at known concentrations. The samples will be injected into the microfluidic device to perform the capture. PCR analysis will indicate the levels of virus in the blood that were not captured. Captured viruses will also be eluted from the fluidic chamber and quantified by PCR, these measurements will be used to calculate capture efficiency. Factors including device geometry and antibody immobilization method will be optimized to achieve consistent high-efficiency capture.
- Liposome production methods will be explored to achieve consistent diameter for a more accurate testing method. Larger liposomes will also be explored and non-specific binding versus liposome size will be characterized to determine the largest allowed liposome size for this assay. The goal will be to improve the lower limit of detection two orders of magnitude.
- Viruses captured from whole blood will be quantified based on the liposome ion release impedance spectroscopy method. Following capture, antibody-functionalized liposomes will be used to tag captured viruses, the device will then be heated and measured to quantify tags, which will indicate the number of captured viruses.
- The fully-integrated device will be testing with clinical specimens from the Carle Foundation Hospital.

Ultimately, the successful completion of this plasma viral load biosensor assay will pave the way for wide application of this ELISA-inspired technique to biomolecule, pathogen and toxin sensing at the point-of-care.

References

[1] WHO, UNAIDS, and UNICEF, "Global HIV/AIDS Response: Epidemic update and health sector progress towards Universal Access," 2011.

[2] United Nations, "Millenium Development Goals," 2012. [Online]. Available: http://www.un.org/millenniumgoals/.

[3] J. a Aberg, J. E. Kaplan, H. Libman, P. Emmanuel, J. R. Anderson, V. E. Stone, J. M. Oleske, J. S. Currier, and J. E. Gallant, "Primary care guidelines for the management of persons infected with human immunodeficiency virus: 2009 update by the HIV medicine Association of the Infectious Diseases Society of America.," *Clinical infectious diseases : an official publication of the Infectious Diseases Society of America*, vol. 49, no. 5, pp. 651–81, Sep. 2009.

[4] G. Pantaleo, C. Graziosi, and A. S. Fauci, "The immunopathogenesis of human immunodeficiency virus infection," *New England Journal of Medicine*, vol. 328, no. 5, pp. 327–335, Feb. 1993.

[5] National Institute of Allergy and Infectious Diseases, "The Relationship Between the Human Immunodeficiency Virus and the Acquired Immunodeficiency Syndrome," *HIV/AIDS*, 2010. [Online]. Available: http://www.niaid.nih.gov/topics/hivaids/understanding/howhivcausesaids/pages/relationshiphivaids.aspx. [Accessed: 12-Apr-2012].

[6] W. H. Organization, "Antiretroviral therapy for HIV infection in adults and adolescents," 2010.

[7] E. M. Krantz, K. H. Hullsiek, J. F. Okulicz, A. C. Weintrob, B. K. Agan, N. F. Crum-Cianflone, A. Ganesan, T. M. Ferguson, and B. R. Hale, "Elevated CD8 counts during HAART are associated with HIV virologic treatment failure.," *JAIDS Journal of Acquired Immune Deficiency Syndromes*, vol. 57, no. 5, pp. 396–403, Aug. 2011.

[8] N. L. Michael, T. Mo, A. Merzouki, M. O. Shaughnessy, C. Oster, D. S. Burke, R. R. Redfield, and D. L. Birx, "Human Immunodeficiency Virus Type 1 Cellular RNA Load and Splicing Patterns Predict Disease Progression in a Longitudinally Studied Cohort," *Journal of Virology*, vol. 69, no. 3, pp. 1868–1877, 1995.

[9] K. Saksela, C. Stevens, and P. Rubinstein, "HIV-1 messenger RNA in peripheral blood mononuclear cells as an early marker of risk for progression to AIDS," *Annals of internal Medicine*, vol. 123, no. 9, 1995.

[10] A. O. Pasternak, S. Jurriaans, M. Bakker, B. Berkhout, and V. V Lukashov, "Steady increase in cellular HIV-1 load during the asymptomatic phase of untreated infection despite stable plasma viremia.," *AIDS*, vol. 24, no. 11, pp. 1641–9, Jul. 2010.

[11] M. R. Furtado and L. A. Kingsley, "Changes in the viral mRNA expression pattern correlate with a rapid rate of CD4 + T-cell number decline in human immunodeficiency virus type 1-infected individuals . Changes in the Viral mRNA Expression Pattern Correlate with a Rapid Rate of CD4 ♀ T-Cell ," 1995.

[12] A. O. Pasternak, S. Jurriaans, M. Bakker, J. M. Prins, B. Berkhout, and V. V Lukashov, “Cellular levels of HIV unspliced RNA from patients on combination antiretroviral therapy with undetectable plasma viremia predict the therapy outcome.,” *PloS one*, vol. 4, no. 12, p. e8490, Dec. 2009.

[13] M. Zanchetta, S. Walker, N. Burighel, D. Bellanova, O. Rampon, C. Giaquinto, and A. De Rossi, “Long-Term Decay of the HIV-1 Reservoir in HIV-1 – Infected Children Treated with Highly Active Antiretroviral Therapy,” vol. 193, 2006.

[14] A. O. Pasternak, K. W. Adema, M. Bakker, S. Jurriaans, B. Berkhout, M. Cornelissen, and V. V Lukashov, “Highly sensitive methods based on seminested real-time reverse transcription-PCR for quantitation of human immunodeficiency virus type 1 unspliced and multiply spliced RNA and proviral DNA.,” *Journal of clinical microbiology*, vol. 46, no. 7, pp. 2206–11, Jul. 2008.

[15] R. S. Soares, P. Matoso, M. Calado, and A. E. Sousa, “Strategies to quantify unspliced and multiply spliced mRNA expression in HIV-2 infection,” *Journal of Virological Methods*, vol. 175, no. 1, pp. 38–45, Jul. 2011.

[16] S. H. Vermund, “Chapter 1: HIV Epidemic,” in *Challenges in Infectious Diseases*, I. W. Fong, Ed. New York, NY: Springer New York, 2013, pp. 3–46.

[17] U.S. Food and Drug Administration, “Complete List of Donor Screening Assays for Infectious Agents and HIV Diagnostic Assays.” .

[18] U.S. Food and Drug Administration, “Vaccines , Blood & Biologics Approved Products: HIV-1,” 2010. [Online]. Available: http://www.fda.gov/BiologicsBloodVaccines/BloodBloodProducts/ApprovedProducts/LicensedProductsBLAs/BloodDonorScreening/InfectiousDisease/ucm126582.htm.

[19] T. Peterson and M. Stuart, “PCR HIV Test,” *Medscape Reference*, 2011. [Online]. Available: http://emedicine.medscape.com/article/1983649-overview.

[20] U.S. Food and Drug Administration and R. Klein, “Three new HIV assays approved,” 2007.

[21] C. Garrido, N. Zahonero, A. Corral, M. Arredondo, V. Soriano, and C. de Mendoza, “Correlation between human immunodeficiency virus type 1 (HIV-1) RNA measurements obtained with dried blood spots and those obtained with plasma by use of Nuclisens EasyQ HIV-1 and Abbott RealTime HIV load tests.,” *Journal of clinical microbiology*, vol. 47, no. 4, pp. 1031–6, Apr. 2009.

[22] A. Johannessen and C. Garrido, “Dried blood spots perform well in viral load monitoring of patients who receive antiretroviral treatment in rural Tanzania,” *Clinical Infectious Diseases*, vol. 49, 2009.

[23] S. Cassol, M. Gill, and R. Pilon, “Quantification of human immunodeficiency virus type 1 RNA from dried plasma spots collected on filter paper.,” *Journal of clinical microbiology*, 1997.

[24] P. Mwaba, S. Cassol, A. Nunn, and R. Pilon, “Whole blood versus plasma spots for measurement of HIV-1 viral load in HIV-infected African patients,” *The Lancet*, vol. 362, no. 9401, pp. 2067–2068, Dec. 2003.

[25] R. de la Rica and M. M. Stevens, “Plasmonic ELISA for the ultrasensitive detection of disease biomarkers with the naked eye,” *Nature Nanotechnology*, no. October, pp. 2–5, Oct. 2012.

[26] C. Jennings and S. Fiscus, “Comparison of two human immunodeficiency virus (HIV) RNA surrogate assays to the standard HIV RNA assay,” *Journal of clinical microbiology*, 2005.

[27] G. Stevens and N. Rekhviashvili, “Evaluation of Two Commercially Available, Inexpensive Alternative Assays Used for Assessing Viral Load in a Cohort of Human Immunodeficiency Virus Type 1 Subtype C-Infected Patients from South Africa,” *Journal of clinical microbiology*, vol. 43, no. 2, pp. 857–861, Feb. 2005.

[28] S. a Fiscus, J. Wiener, E. J. Abrams, M. Bulterys, A. Cachafeiro, and R. a Respess, “Ultrasensitive p24 antigen assay for diagnosis of perinatal human immunodeficiency virus type 1 infection.,” *Journal of clinical microbiology*, vol. 45, no. 7, pp. 2274–7, Jul. 2007.

[29] R. Respess and A. Cachafeiro, “Evaluation of an ultrasensitive p24 antigen assay as a potential alternative to human immunodeficiency virus type 1 RNA viral load assay in resource-limited settings,” *Journal of clinical microbiology*, 2005.

[30] D. Bonard, F. Rouet, T. Toni, and A. Minga, “Field evaluation of an improved assay using a heat-dissociated p24 antigen for adults mainly infected with HIV-1 CRF02_AG strains in Cote d’Ivoire, West Africa.,” *JAIDS Journal of Acquired Immune Deficiency Syndromes*, 2003.

[31] K. Steegen, S. Luchters, N. De Cabooter, J. Reynaerts, K. Mandaliya, J. Plum, W. Jaoko, C. Verhofstede, and M. Temmerman, “Evaluation of two commercially available alternatives for HIV-1 viral load testing in resource-limited settings.,” *Journal of virological methods*, vol. 146, no. 1–2, pp. 178–87, Dec. 2007.

[32] K.-B. Lee, E.-Y. Kim, C. a. Mirkin, and S. M. Wolinsky, “The Use of Nanoarrays for Highly Sensitive and Selective Detection of Human Immunodeficiency Virus Type 1 in Plasma,” *Nano Lett.*, vol. 4, no. 10, pp. 1869–1872, Oct. 2004.

[33] Z. a Parpia, R. Elghanian, A. Nabatiyan, D. R. Hardie, and D. M. Kelso, “p24 antigen rapid test for diagnosis of acute pediatric HIV infection.,” *JAIDS Journal of Acquired Immune Deficiency Syndromes*, vol. 55, no. 4, pp. 413–9, Dec. 2010.

[34] S. Tang, J. Zhao, and J. Storhoff, “Nanoparticle-based biobarcode amplification assay (BCA) for sensitive and early detection of human immunodeficiency type 1 capsid (p24) antigen,” *JAIDS Journal of Acquired Immune Deficiency Syndromes*, vol. 46, no. 2, pp. 231–237, Oct. 2007.

[35] S. Tang and I. Hewlett, “Nanoparticle-based immunoassays for sensitive and early detection of HIV-1 capsid (p24) antigen.,” *The Journal of infectious diseases*, vol. 201 Suppl , no. Suppl 1, pp. S59–64, Apr. 2010.

[36] E. Kim, J. Stanton, and B. Korber, “Detection of HIV-1 p24 Gag in plasma by a nanoparticle-based bio-barcode-amplification method,” *Nanomedicine*, vol. 3, no. 3, 2008.

[37] J. Nam, C. Thaxton, and C. Mirkin, “Nanoparticle-based bio-bar codes for the ultrasensitive detection of proteins,” *Science*, vol. 301, no. 5641, pp. 1884–1886, Sep. 2003.

[38] D. H. Ekstrand, R. J. Awad, C. F. Källander, and J. S. Gronowitz, “A sensitive assay for the quantification of reverse transcriptase activity based on the use of carrier-bound template and non-radioactive-product detection, with special reference to human-immunodeficiency-virus isolation.,” *Biotechnology and applied biochemistry*, vol. 23 (Pt 2), pp. 95–105, Apr. 1996.

[39] A. Malmsten, X.-W. Shao, K. Aperia, G. E. Corrigan, E. Sandström, C. F. R. Källander, T. Leitner, and J. S. Gronowitz, “HIV-1 viral load determination based on reverse transcriptase activity recovered from human plasma.,” *Journal of medical virology*, vol. 71, no. 3, pp. 347–59, Nov. 2003.

[40] A. Malmsten, X.-W. Shao, S. Sjödahl, E.-L. Fredriksson, I. Pettersson, T. Leitner, C. F. R. Källander, E. Sandström, and J. S. Gronowitz, “Improved HIV-1 viral load determination based on reverse transcriptase activity recovered from human plasma.,” *Journal of medical virology*, vol. 76, no. 3, pp. 291–6, Jul. 2005.

[41] J. Lombart, M. Vray, and A. Kafando, “Plasma virion reverse transcriptase activity and heat dissociation-boosted p24 assay for HIV load in Burkina Faso, West Africa,” *Aids*, no. April, pp. 1273–1277, 2005.

[42] M. Mine, K. Bedi, T. Maruta, D. Madziva, M. Tau, T. Zana, T. Gaolathe, S. Moyo, K. Seipone, N. Ndwapi, M. Essex, and R. Marlink, “Quantitation of human immunodeficiency virus type 1 viral load in plasma using reverse transcriptase activity assay at a district hospital laboratory in Botswana: a decentralization pilot study.,” *Journal of virological methods*, vol. 159, no. 1, pp. 93–7, Jul. 2009.

[43] V. Greengrass, B. Lohman, L. Morris, M. Plate, P. M. Steele, J. L. Walson, and S. M. Crowe, “Assessment of the low-cost Cavidi ExaVir Load assay for monitoring HIV viral load in pediatric and adult patients.,” *JAIDS Journal of Acquired Immune Deficiency Syndromes*, vol. 52, no. 3, pp. 387–90, Nov. 2009.

[44] J. Braun, J.-C. Plantier, M.-F. Hellot, E. Tuaillon, M. Gueudin, F. Damond, A. Malmsten, G. E. Corrigan, and F. Simon, “A new quantitative HIV load assay based on plasma virion reverse transcriptase activity for the different types, groups and subtypes.,” *AIDS*, vol. 17, no. 3, pp. 331–6, Feb. 2003.

[45] S. Sivapalasingam and S. Essajee, “Human immunodeficiency virus (HIV) reverse transcriptase activity correlates with HIV RNA load: implications for resource-limited settings,” *Journal of clinical microbiology*, 2005.

[46] H. S. Iqbal, P. Balakrishnan, A. J. Cecelia, S. Solomon, N. Kumarasamy, V. Madhavan, K. G. Murugavel, A. K. Ganesh, S. S. Solomon, K. H. Mayer, and S. M. Crowe, “Use of an HIV-1 reverse-transcriptase enzyme-activity assay to measure HIV-1 viral load as a potential alternative to nucleic acid-based assay for monitoring antiretroviral therapy in resource-limited settings,” *Journal of medical microbiology*, vol. 56, no. 12, pp. 1611–4, Dec. 2007.

[47] V. L. Greengrass, M. M. Plate, P. M. Steele, J. T. Denholm, C. L. Cherry, L. M. Morris, A. Hearps, and S. M. Crowe, "Evaluation of the Cavidi ExaVir Load assay (version 3) for plasma human immunodeficiency virus type 1 load monitoring.," *Journal of clinical microbiology*, vol. 47, no. 9, pp. 3011–3, Sep. 2009.

[48] W. Labbett, A. Garcia-Diaz, Z. Fox, G. S. Clewley, T. Fernandez, M. Johnson, and A. M. Geretti, "Comparative evaluation of the ExaVir Load version 3 reverse transcriptase assay for measurement of human immunodeficiency virus type 1 plasma load.," *Journal of clinical microbiology*, vol. 47, no. 10, pp. 3266–70, Oct. 2009.

[49] P. Stewart, A. Cachafeiro, S. Napravnik, J. J. Eron, I. Frank, C. van der Horst, R. J. Bosch, D. Bettendorf, P. Bohlin, and S. a Fiscus, "Performance characteristics of the Cavidi ExaVir viral load assay and the ultra-sensitive P24 assay relative to the Roche Monitor HIV-1 RNA assay.," *Journal of clinical virology*, vol. 49, no. 3, pp. 198–204, Nov. 2010.

[50] W. Tang, W. H. a Chow, Y. Li, H. Kong, Y.-W. Tang, and B. Lemieux, "Nucleic acid assay system for tier II laboratories and moderately complex clinics to detect HIV in low-resource settings.," *The Journal of infectious diseases*, vol. 201 Suppl, no. Suppl 1, pp. S46–51, Apr. 2010.

[51] H. H. Lee, M. a Dineva, Y. L. Chua, A. V Ritchie, I. Ushiro-Lumb, and C. a Wisniewski, "Simple amplification-based assay: a nucleic acid-based point-of-care platform for HIV-1 testing.," *The Journal of infectious diseases*, vol. 201 Suppl, no. Suppl 1, pp. S65–72, Apr. 2010.

[52] S. H. Lee, S.-W. Kim, J. Y. Kang, and C. H. Ahn, "A polymer lab-on-a-chip for reverse transcription (RT)-PCR based point-of-care clinical diagnostics.," *Lab on a chip*, vol. 8, no. 12, pp. 2121–7, Dec. 2008.

[53] F. Shen, B. Sun, J. E. Kreutz, E. K. Davydova, W. Du, P. L. Reddy, L. J. Joseph, and R. F. Ismagilov, "Multiplexed quantification of nucleic acids with large dynamic range using multivolume digital RT-PCR on a rotational SlipChip tested with HIV and hepatitis C viral load.," *Journal of the American Chemical Society*, vol. 133, no. 44, pp. 17705–12, Nov. 2011.

[54] B. A. Rohrman, V. Leautaud, E. Molyneux, and R. R. Richards-Kortum, "A Lateral Flow Assay for Quantitative Detection of Amplified HIV-1 RNA," *PLoS ONE*, vol. 7, no. 9, pp. e45611–e45611, Sep. 2012.

[55] S. Tanriverdi, L. Chen, and S. Chen, "A rapid and automated sample-to-result HIV load test for near-patient application," *The Journal of infectious diseases*, vol. 201 Suppl, no. s1, pp. S52–8, Apr. 2010.

[56] Y.-G. Kim, S. Moon, D. R. Kuritzkes, and U. Demirci, "Quantum dot-based HIV capture and imaging in a microfluidic channel.," *Biosensors and Bioelectronics*, vol. 25, no. 1, pp. 253–8, Sep. 2009.

[57] S. Wang, A. Ip, F. Xu, F. F. Giguel, S. Moon, A. Akay, D. R. Kuritzkes, and U. Demirci, "Development of a microfluidic system for measuring HIV-1 viral load," *Sensors, and Command, Control, Communications, and Intelligence (C3I) Technologies for Homeland Security and Homeland Defense IX*, vol. 7666, p. 76661H–76661H–6, Apr. 2010.

[58] S. Wang, M. Esfahani, U. a Gurkan, F. Inci, D. R. Kuritzkes, and U. Demirci, "Efficient on-chip isolation of HIV subtypes.," *Lab on a chip*, vol. 12, no. 8, pp. 1508–15, Mar. 2012.

[59] G. Chen, C. J. Alberts, W. Rodriguez, and M. Toner, "Concentration and purification of human immunodeficiency virus type 1 virions by microfluidic separation of superparamagnetic nanoparticles.," *Analytical chemistry*, vol. 82, no. 2, pp. 723–8, Jan. 2010.

[60] S. Cassol, A. Butcher, and S. Kinard, "Rapid screening for early detection of mother-to-child transmission of human immunodeficiency virus type 1.," *Journal of clinical microbiology*, pp. 1–6, 1994.

[61] J. Weidner, U. Cassens, W. Göhde, W. Sibrowski, G. Odaibo, D. Olaleye, D. Reichelt, and B. Greve, "An improved PCR method for detection of HIV-1 proviral DNA of a wide range of subtypes and recombinant forms circulating globally," *Journal of Virological Methods*, vol. 172, no. 1–2, pp. 22–26, Mar. 2011.

[62] T. E. Schutzbank and J. Smith, "Detection of human immunodeficiency virus type 1 proviral DNA by PCR using an electrochemiluminescence-tagged probe.," *Journal of clinical microbiology*, vol. 33, no. 8, pp. 2036–41, Aug. 1995.

[63] D. Zella, A. Cavicchini, and E. Cattaneo, "Utilization of a DNA enzyme immunoassay for the detection of proviral DNA of human immunodeficiency virus type 1 by polymerase chain reaction," *Clinical and Diagnostic Virology*, vol. 3, no. 2, pp. 155–164, Feb. 1995.

[64] K. L. Barlow, J. H. C. Tosswill, J. V Parry, and J. P. Clewley, "Performance of the Amplicor Human Immunodeficiency Virus Type 1 PCR and Analysis of Specimens with False-Negative Results," vol. 35, no. 11, pp. 2846–2853, 1997.

[65] J. W. Bremer, J. F. Lew, E. Cooper, G. V Hillyer, J. Pitt, E. Handelsman, D. Brambilla, J. Moye, and R. Haft, "Diagnosis of infection with human immunodeficiency virus type 1 by a DNA polymerase chain reaction assay among infants enrolled in the Women and Infants ' Transmission Study," 1996.

[66] C. Delamare, M. Burgard, and M. Mayaux, "HIV-1 RNA detection in plasma for the diagnosis of infection in neonates," *JAIDS Journal of*, vol. 15, no. 2, pp. 121–125, 1997.

[67] CDC, "HIV Testing Basics for Consumers," *HIV Testing Basics for Consumers*, 2010. [Online]. Available: http://www.cdc.gov/hiv/topics/testing/resources/qa/index.htm.

[68] C. Christopherson, Y. Kidane, B. Conway, H. Sheppard, S. Kwok, and J. Krowka, "PCR-Based Assay To Quantify Human Immunodeficiency Virus Type 1 DNA in Peripheral Blood Mononuclear Cells These include : PCR-Based Assay To Quantify Human Immunodeficiency Virus Type 1 DNA in Peripheral Blood Mononuclear Cells," 2000.

[69] N. Désiré, A. Dehée, V. Schneider, C. Jacomet, C. Goujon, P. Girard, W. Rozenbaum, and J. Nicolas, "Quantification of Human Immunodeficiency Virus Type 1 Proviral Load by a TaqMan Real-Time PCR Assay Quantification of Human Immunodeficiency Virus Type 1 Proviral Load by a TaqMan Real-Time PCR Assay," 2001.

[70] L. G. Kostrikis, G. Touloumi, R. Karanicolas, N. Pantazis, C. Anastassopoulou, J. J. Goedert, A. Hatzakis, and A. Karafoulidou, "Quantitation of Human Immunodeficiency Virus Type 1 DNA Forms with the Second Template Switch in Peripheral Blood Cells Predicts Disease Progression Independently of Plasma RNA Load Quantitation of Human Immunodeficiency Virus Type 1 DNA Forms with the Se," 2002.

[71] A. E. Hatzakis, G. Touloumi, N. Pantazis, C. G. Anastassopoulou, O. Katsarou, A. Karafoulidou, J. J. Goedert, and L. G. Kostrikis, "Cellular HIV-1 DNA load predicts HIV-RNA rebound and the outcome of highly active antiretroviral therapy," no. September, 2004.

[72] D. Gibellini, M. Borderi, E. De Crignis, R. Cicola, L. Cimatti, F. Vitone, F. Chiodo, and M. C. Re, "HIV-1 DNA load analysis in peripheral blood lymphocytes and monocytes from naïve and HAART-treated individuals.," *Journal of Infection*, vol. 56, no. 3, pp. 219–25, Mar. 2008.

[73] M. C. Re, F. Vitone, C. Biagetti, P. Schiavone, F. Alessandrini, I. Bon, E. de Crignis, and D. Gibellini, "HIV-1 DNA proviral load in treated and untreated HIV-1 seropositive patients.," *Clinical microbiology and infection : the official publication of the European Society of Clinical Microbiology and Infectious Diseases*, vol. 16, no. 6, pp. 640–6, Jun. 2010.

[74] S. M. Moroney, L. C. Heller, and R. H. Widen, "Evaluation of two TaqMan PCR assays for the detection of HIV-1 proviral DNA in blood samples," *Journal of Microbiological Methods*, vol. 65, no. 2, pp. 350–353, May 2006.

[75] M. S. Malnati, G. Scarlatti, F. Gatto, F. Salvatori, G. Cassina, T. Rutigliano, R. Volpi, and P. Lusso, "A universal real-time PCR assay for the quantification of group-M HIV-1 proviral load.," *Nature protocols*, vol. 3, no. 7, pp. 1240–8, Jul. 2008.

[76] A. De Rossi, M. Zanchetta, F. Vitone, G. Antonelli, P. Bagnarelli, L. Buonaguro, M. R. Capobianchi, M. Clementi, I. Abbate, F. Canducci, A. Monachetti, E. Riva, G. Rozera, C. Scagnolari, M. Tagliamonte, M. Carla, and I. Society, "Quantitative HIV-1 proviral DNA detection : a multicentre analysis," pp. 293–302, 2010.

[77] S. R. Jangam, D. H. Yamada, S. M. McFall, and D. M. Kelso, "Rapid, point-of-care extraction of human immunodeficiency virus type 1 proviral DNA from whole blood for detection by real-time PCR.," *Journal of clinical microbiology*, vol. 47, no. 8, pp. 2363–8, Aug. 2009.

[78] S. R. Jangam, A. K. Agarwal, K. Sur, and D. M. Kelso, "A point-of-care PCR test for HIV-1 detection in resource-limited settings," *Biosensors and Bioelectronics*, Oct. 2012.

[79] J.-H. Wang, L. Cheng, C.-H. Wang, W.-S. Ling, S.-W. Wang, and G.-B. Lee, "An integrated chip capable of performing sample pretreatment and nucleic acid amplification for HIV-1 detection," *Biosensors and Bioelectronics*, Sep. 2012.

[80] S. Y. Bae, H. C. Park, J. S. Oh, S.-Y. Yoon, D. W. Park, I. K. Choi, H. J. Kim, J. H. Oh, D. S. Hur, C. Chung, J. K. Chang, J. P. Robinson, and C. S. Lim, "Absolute CD4 cell count using a plastic microchip and a microscopic cell counter.," *Cytometry*, vol. 76B, no. 5, pp. 345–53, Sep. 2009.

[81] W. R. Rodriguez, N. Christodoulides, P. N. Floriano, S. Graham, S. Mohanty, M. Dixon, M. Hsiang, T. Peter, S. Zavahir, I. Thior, D. Romanovicz, B. Bernard, A. P. Goodey, B. D. Walker,

and J. T. McDevitt, “A microchip CD4 counting method for HIV monitoring in resource-poor settings.,” *PLoS medicine*, vol. 2, no. 7, p. e182, Jul. 2005.

[82] M. a Alyassin, S. Moon, H. O. Keles, F. Manzur, R. L. Lin, E. Hæggstrom, D. R. Kuritzkes, and U. Demirci, “Rapid automated cell quantification on HIV microfluidic devices.,” *Lab on a chip*, vol. 9, no. 23, pp. 3364–9, Dec. 2009.

[83] S. Thorslund, R. Larsson, F. Nikolajeff, J. Bergquist, and J. Sanchez, “Bioactivated PDMS microchannel evaluated as sensor for human CD4+ cells—The concept of a point-of-care method for HIV monitoring,” *Sensors and Actuators B Chemical*, vol. 123, no. 2, pp. 847–855, May 2007.

[84] S. Thorslund, R. Larsson, J. Bergquist, F. Nikolajeff, and J. Sanchez, “A PDMS-based disposable microfluidic sensor for CD4+ lymphocyte counting,” *Biomedical microdevices*, vol. 10, no. 6, pp. 851–7, Dec. 2008.

[85] J. V Jokerst, J. W. Jacobson, B. D. Bhagwandin, P. N. Floriano, N. Christodoulides, and J. T. McDevitt, “Programmable nano-bio-chip sensors: analytical meets clinical.,” *Analytical chemistry*, vol. 82, no. 5, pp. 1571–9, Mar. 2010.

[86] J. V Jokerst, P. N. Floriano, N. Christodoulides, G. W. Simmons, and J. T. McDevitt, “Integration of semiconductor quantum dots into nano-bio-chip systems for enumeration of CD4+ T cell counts at the point-of-need.,” *Lab on a chip*, vol. 8, no. 12, pp. 2079–90, Dec. 2008.

[87] X. Li, A. Ymeti, B. Lunter, C. Breukers, A. G. J. Tibbe, L. W. M. M. Terstappen, and J. Greve, “CD4+ T lymphocytes enumeration by an easy-to-use single platform image cytometer for HIV monitoring in resource-constrained settings,” *Cytometry*, vol. 72B, no. 5, pp. 397–407, Sep. 2007.

[88] A. Ymeti, X. Li, B. Lunter, and C. Breukers, “A single platform image cytometer for resource-poor settings to monitor disease progression in HIV infection,” *Cytometry*, vol. 71A, no. 3, pp. 132–142, Mar. 2007.

[89] X. Li, A. G. J. Tibbe, E. Droog, L. W. M. M. Terstappen, and J. Greve, “An immunomagnetic single-platform image cytometer for cell enumeration based on antibody specificity.,” *Clinical and Vaccine Immunology*, vol. 14, no. 4, pp. 412–9, Apr. 2007.

[90] X. Cheng, D. Irimia, M. Dixon, K. Sekine, U. Demirci, L. Zamir, R. G. Tompkins, W. Rodriguez, and M. Toner, “A microfluidic device for practical label-free CD4(+) T cell counting of HIV-infected subjects.,” *Lab on a chip*, vol. 7, no. 2, pp. 170–8, Feb. 2007.

[91] X. Cheng, D. Irimia, M. Dixon, J. C. Ziperstein, U. Demirci, L. Zamir, R. G. Tompkins, M. Toner, and W. R. Rodriguez, “A microchip approach for practical label-free CD4+ T-cell counting of HIV-infected subjects in resource-poor settings,” *JAIDS Journal of Acquired Immune Deficiency Syndromes*, vol. 45, no. 3, p. 257, 2007.

[92] X. Cheng, A. Gupta, C. Chen, R. G. Tompkins, W. Rodriguez, and M. Toner, “Enhancing the performance of a point-of-care CD4+ T-cell counting microchip through monocyte depletion for HIV/AIDS diagnostics.,” *Lab on a chip*, vol. 9, no. 10, pp. 1357–64, May 2009.

[93] M. Beck, S. Brockhuis, N. van der Velde, C. Breukers, J. Greve, and L. W. M. M. Terstappen, "On-chip sample preparation by controlled release of antibodies for simple CD4 counting.," *Lab on a chip*, vol. 12, no. 1, pp. 167–73, Jan. 2012.

[94] C. D. Chin, V. Linder, and S. K. Sia, "Commercialization of microfluidic point-of-care diagnostic devices," *Lab on a chip*, vol. 12, no. 12, pp. 2118–34, Jun. 2012.

[95] S. Mtapuri-Zinyowera, M. Chideme, D. Mangwanya, O. Mugurungi, S. Gudukeya, K. Hatzold, A. Mangwiro, G. Bhattacharya, J. Lehe, and T. Peter, "Evaluation of the PIMA point-of-care CD4 analyzer in VCT clinics in Zimbabwe.," *JAIDS Journal of Acquired Immune Deficiency Syndromes*, vol. 55, no. 1, pp. 1–7, Sep. 2010.

[96] I. V Jani, N. E. Sitoe, P. L. Chongo, E. R. Alfai, J. I. Quevedo, O. Tobaiwa, J. D. Lehe, and T. F. Peter, "Accurate CD4 T-cell enumeration and antiretroviral drug toxicity monitoring in primary healthcare clinics using point-of-care testing.," *AIDS*, vol. 25, no. 6, pp. 807–12, Mar. 2011.

[97] B. Larson, K. Schnippel, B. Ndibongo, L. Long, M. P. Fox, and S. Rosen, "How to Estimate the Cost of Point-of-Care CD4 Testing in Program Settings: An Example Using the Alere Pima Analyzer in South Africa," *PloS one*, vol. 7, no. 4, p. e35444, Apr. 2012.

[98] Y. C. Manabe, Y. Wang, A. Elbireer, B. Auerbach, and B. Castelnuovo, "Evaluation of portable point-of-care CD4 counter with high sensitivity for detecting patients eligible for antiretroviral therapy," *PloS one*, vol. 7, no. 4, p. e34319, Apr. 2012.

[99] S. Herbert, S. Edwards, G. Carrick, A. Copas, C. Sandford, M. Amphlett, and P. Benn, "Evaluation of PIMA point-of-care CD4 testing in a large UK HIV service.," *Sexually transmitted infections*, vol. 88, no. 6, pp. 413–7, Oct. 2012.

[100] I. Jani, N. Sitoe, J. Quevedo, J. Lehe, and T. Peter, "Cost comparison of point-of-care and laboratory CD4 testing in resource-limited settings," in *6th IAS Conference on HIV Pathogenesis, Treatment and Prevention*, 2011.

[101] J. T. Gohring and X. Fan, "Label free detection of CD4+ and CD8+ T cells using the optofluidic ring resonator.," *Sensors*, vol. 10, no. 6, pp. 5798–808, Jun. 2010.

[102] S. Moon, H. O. Keles, A. Ozcan, A. Khademhosseini, E. Haeggstrom, D. Kuritzkes, and U. Demirci, "Integrating microfluidics and lensless imaging for point-of-care testing.," *Biosensors and Bioelectronics*, vol. 24, no. 11, pp. 3208–14, Jul. 2009.

[103] A. Ozcan and U. Demirci, "Ultra wide-field lens-free monitoring of cells on-chip.," *Lab on a chip*, vol. 8, no. 1, pp. 98–106, Jan. 2008.

[104] Z. Wang, S. Chin, C. Chin, and J. Sarik, "Microfluidic CD4+ T-cell counting device using chemiluminescence-based detection," *Analytical Chemistry*, vol. 82, no. 1, pp. 36–40, Jan. 2010.

[105] S. Moon, U. A. Gurkan, J. Blander, W. W. Fawzi, S. Aboud, F. Mugusi, D. R. Kuritzkes, and U. Demirci, "Enumeration of CD4+ T-cells using a portable microchip count platform in Tanzanian HIV-infected patients," *PloS one*, vol. 6, no. 7, p. e21409, Jul. 2011.

[106] N. Mishra and S. Retterer, “Bio-impedance sensing device (BISD) for detection of human CD4+ cells,” *... Proceedings of the ...*, pp. 228–231, 2004.

[107] N. N. Mishra, S. Retterer, T. J. Zieziulewicz, M. Isaacson, D. Szarowski, D. E. Mousseau, D. a Lawrence, and J. N. Turner, “On-chip micro-biosensor for the detection of human CD4+ cells based on AC impedance and optical analysis,” *Biosensors and Bioelectronics*, vol. 21, no. 5, pp. 696–704, Nov. 2005.

[108] X. Jiang and M. G. Spencer, “Electrochemical impedance biosensor with electrode pixels for precise counting of CD4+ cells: a microchip for quantitative diagnosis of HIV infection status of AIDS patients.,” *Biosensors and Bioelectronics*, vol. 25, no. 7, pp. 1622–8, Mar. 2010.

[109] X. Cheng, Y. Liu, D. Irimia, U. Demirci, L. Yang, L. Zamir, W. R. Rodríguez, M. Toner, and R. Bashir, “Cell detection and counting through cell lysate impedance spectroscopy in microfluidic devices.,” *Lab on a chip*, vol. 7, no. 6, pp. 746–55, Jun. 2007.

[110] P. Kiesel, M. Beck, and N. Johnson, “Monitoring CD4 in whole blood with an opto-fluidic detector based on spatially modulated fluorescence emission.,” *Cytometry*, vol. 79A, no. 4, pp. 317–24, Apr. 2011.

[111] J.-H. Wang, C.-H. Wang, C.-C. Lin, H.-Y. Lei, and G.-B. Lee, “An integrated microfluidic system for counting of CD4+/CD8+ T lymphocytes,” *Microfluidics and Nanofluidics*, vol. 10, no. 3, pp. 531–541, Mar. 2011.

[112] H. Yun, H. Bang, J. Min, C. Chung, J. K. Chang, and D.-C. Han, “Simultaneous counting of two subsets of leukocytes using fluorescent silica nanoparticles in a sheathless microchip flow cytometer.,” *Lab on a chip*, vol. 10, no. 23, pp. 3243–54, Dec. 2010.

[113] X. Mao, S.-C. S. Lin, C. Dong, and T. J. Huang, “Single-layer planar on-chip flow cytometer using microfluidic drifting based three-dimensional (3D) hydrodynamic focusing.,” *Lab on a chip*, vol. 9, no. 11, pp. 1583–9, Jun. 2009.

[114] Y.-N. Wang, Y. Kang, D. Xu, C. H. Chon, L. Barnett, S. a Kalams, D. Li, and D. Li, “On-chip counting the number and the percentage of CD4+ T lymphocytes.,” *Lab on a chip*, vol. 8, no. 2, pp. 309–15, Feb. 2008.

[115] X. Wu, Y. Kang, Y.-N. Wang, D. Xu, D. Li, and D. Li, “Microfluidic differential resistive pulse sensors.,” *Electrophoresis*, vol. 29, no. 13, pp. 2754–9, Jul. 2008.

[116] X. Wu, C. H. Chon, Y.-N. Wang, Y. Kang, and D. Li, “Simultaneous particle counting and detecting on a chip.,” *Lab on a chip*, vol. 8, no. 11, pp. 1943–9, Nov. 2008.

[117] D. Holmes, D. Pettigrew, C. H. C. H. Reccius, J. D. Gwyer, C. van Berkel, J. Holloway, D. E. Davies, H. Morgan, C. Van Berkel, and D. Morganti, “Leukocyte analysis and differentiation using high speed microfluidic single cell impedance cytometry,” *Lab on a chip*, vol. 9, no. 20, pp. 2881–9, Oct. 2009.

[118] C. van Berkel, J. D. Gwyer, S. Deane, N. G. Green, J. Holloway, V. Hollis, and H. Morgan, "Integrated systems for rapid point of care (PoC) blood cell analysis," *Lab on a chip*, vol. 11, no. 7, pp. 1249–55, Apr. 2011.

[119] D. Holmes and H. Morgan, "Single cell impedance cytometry for identification and counting of CD4 T-cells in human blood using impedance labels.," *Analytical Chemistry*, vol. 82, no. 4, pp. 1455–61, Feb. 2010.

[120] N. Watkins, B. M. Venkatesan, M. Toner, W. Rodriguez, and R. Bashir, "A robust electrical microcytometer with 3-dimensional hydrofocusing.," *Lab on a chip*, vol. 9, no. 22, pp. 3177–84, Nov. 2009.

[121] N. N. Watkins, S. Sridhar, X. Cheng, G. D. Chen, M. Toner, W. Rodriguez, and R. Bashir, "A microfabricated electrical differential counter for the selective enumeration of CD4+ T lymphocytes.," *Lab on a chip*, vol. 11, no. 8, pp. 1437–47, Apr. 2011.

[122] H. Zhu, J. Yan, and A. Revzin, "Catch and release cell sorting: electrochemical desorption of T-cells from antibody-modified microelectrodes.," *Colloids and Surfaces B Biointerfaces*, vol. 64, no. 2, pp. 260–8, Jul. 2008.

[123] J. Robertus, W. R. Browne, and B. L. Feringa, "Dynamic control over cell adhesive properties using molecular-based surface engineering strategies.," *Chemical Society reviews*, vol. 39, no. 1, pp. 354–78, Jan. 2010.

[124] U. A. Gurkan, T. Anand, H. Tas, D. Elkan, A. Akay, H. O. Keles, and U. Demirci, "Controlled viable release of selectively captured label-free cells in microchannels," *Lab on a Chip*, vol. 11, no. 23, pp. 3979–3989, Dec. 2011.

[125] C. Willyard, "Simpler tests for immune cells could transform AIDS care in Africa.," *Nature medicine*, vol. 13, no. 10, p. 1131, Oct. 2007.

[126] D. S. Boyle, K. R. Hawkins, M. S. Steele, M. Singhal, and X. Cheng, "Emerging technologies for point-of-care CD4 T-lymphocyte counting.," *Trends in biotechnology*, vol. 30, no. 1, pp. 45–54, Jan. 2012.

[127] R. Zachariah, S. D. Reid, P. Chaillet, M. Massaquoi, E. J. Schouten, and a D. Harries, "Viewpoint: Why do we need a point-of-care CD4 test for low-income countries?," *Tropical medicine & international health : TM & IH*, vol. 16, no. 1, pp. 37–41, Jan. 2011.

[128] M. Kitahata and S. Gange, "Effect of early versus deferred antiretroviral therapy for HIV on survival," *New England Journal of Medicine*, pp. 1815–1826, 2009.

[129] D. D. Ho, "Viral counts count in HIV infection," *Science*, vol. 272, no. 5265, p. 1124, 1996.

[130] G. L. Damhorst, N. N. Watkins, and R. Bashir, "Micro- and Nanotechnology for HIV/AIDS Diagnostics in Resource-Limited Settings.," *IEEE transactions on bio-medical engineering*, vol. 60, no. 3, pp. 715–26, Mar. 2013.

[131] R. Gómez-sjöberg, D. T. Morisette, R. Bashir, and S. Member, "Impedance Microbiology-on-a-Chip : Microfluidic Bioprocessor for Rapid Detection of Bacterial Metabolism," *Journal of Microelectromechanical Systems*, vol. 14, no. 4, pp. 829–838, 2005.

[132] R. Gómez, R. Bashir, and A. Bhunia, "Microscale electronic detection of bacterial metabolism," *Sensors and Actuators B: Chemical*, vol. 86, pp. 198–208, 2002.

[133] F. Lisdat and D. Schäfer, "The use of electrochemical impedance spectroscopy for biosensing.," *Analytical and bioanalytical chemistry*, vol. 391, no. 5, pp. 1555–67, Jul. 2008.

[134] H. Shafiee, M. Jahangir, F. Inci, S. Wang, R. B. M. Willenbrecht, F. F. Giguel, A. M. N. Tsibris, D. R. Kuritzkes, and U. Demirci, "Acute On-Chip HIV Detection Through Label-Free Electrical Sensing of Viral Nano-Lysate.," *Small*, pp. 1–11, Feb. 2013.

[135] J. T. Connelly, S. Kondapalli, M. Skoupi, J. S. L. Parker, B. J. Kirby, and A. J. Baeumner, "Micro-total analysis system for virus detection: microfluidic pre-concentration coupled to liposome-based detection.," *Analytical and bioanalytical chemistry*, vol. 402, no. 1, pp. 315–23, Jan. 2012.

[136] S. Kwakye, V. N. Goral, and A. J. Baeumner, "Electrochemical microfluidic biosensor for nucleic acid detection with integrated minipotentiostat.," *Biosensors and Bioelectronics*, vol. 21, no. 12, pp. 2217–23, Jun. 2006.

[137] K. a Edwards, O. R. Bolduc, and A. J. Baeumner, "Miniaturized bioanalytical systems: enhanced performance through liposomes.," *Current opinion in chemical biology*, pp. 1–9, Jun. 2012.

[138] S. R. Nugen, P. J. Asiello, J. T. Connelly, and A. J. Baeumner, "PMMA biosensor for nucleic acids with integrated mixer and electrochemical detection.," *Biosensors and Bioelectronics*, vol. 24, no. 8, pp. 2428–33, Apr. 2009.

[139] Q. Liu and B. Boyd, "Liposomes in biosensors," *Analyst*, no. 207890, 2012.

[140] N. V Zaytseva, V. N. Goral, R. a Montagna, and A. J. Baeumner, "Development of a microfluidic biosensor module for pathogen detection.," *Lab on a chip*, vol. 5, no. 8, pp. 805–11, Aug. 2005.

[141] N. V Zaytseva, R. a Montagna, and A. J. Baeumner, "Microfluidic biosensor for the serotype-specific detection of dengue virus RNA.," *Analytical chemistry*, vol. 77, no. 23, pp. 7520–7, Dec. 2005.

[142] "Technical Conductivity and Resistivity," *Omega Engineering, Inc.* [Online]. Available: http://www.omega.com/techref/ph-2.html.

[143] CSM, "Conductivity of Alkali Solution," *Technology Express CSM*. [Online]. Available: http://www.csmfilter.com/csm/upload/TechManual/ConductivitySalt.pdf.

[144] S. a Kim and J. S. Peacock, "The use of palmitate-conjugated protein A for coating cells with artificial receptors which facilitate intercellular interactions.," *Journal of immunological methods*, vol. 158, no. 1, pp. 57–65, Jan. 1993.

[145] T. Chen, D. McIntosh, Y. He, J. Kim, D. a Tirrell, P. Scherrer, D. B. Fenske, A. P. Sandhu, and P. R. Cullis, "Alkylated derivatives of poly(ethylacrylic acid) can be inserted into preformed liposomes and trigger pH-dependent intracellular delivery of liposomal contents.," *Molecular membrane biology*, vol. 21, no. 6, pp. 385–93, 2004.

[146] M. Hwang, R. Prud'homme, J. Kohn, and J. Thomas, "Stabilization of phosphatidylserine/phosphatidylethanolamine liposomes with hydrophilic polymers having multiple 'Sticky Feet'," *Langmuir*, vol. 17, no. 25, 2001.

[147] S.-Y. Teh, R. Khnouf, H. Fan, and A. P. Lee, "Stable, biocompatible lipid vesicle generation by solvent extraction-based droplet microfluidics.," *Biomicrofluidics*, vol. 5, no. 4, pp. 44113–4411312, Dec. 2011.

[148] A. deMello and D. van Swaay, "Microfluidic methods for forming liposomes," *Lab on a Chip*, 2012.

Appendix A: Impedance sensor fabrication protocol

Double resist metal lift-off recipe

1. Piranha clean (Sulfuric Acid:Hydrogen Peroxide::1:1), 15 minutes; rinse 10 minutes; nitrogen dry.
2. Dehydration bake @ 110 C, 5 minutes minimum; 5 minutes cool-off.
3. Spin LOR 3A (put on enough LOR 3A to cover entire wafer before spinning; this helps chip yield greatly)
    a. 0 to 500 rpm in 1 s (acceleration setting)
    b. hold at 500 rpm for 2 s
    c. 500 to 3000 rpm in 2 s (acceleration setting)
    d. hold at 3000 rpm for 35 s
4. Soft bake: 5 min. @ 183 C (directly on hotplate, not with metal holders); 5 minutes cool off
5. Spin S1805 (put on enough S1805 to cover entire wafer, not just 4 mL)
    a. 0 to 500 rpm in 1 s (acceleration setting)
    b. hold at 500 rpm for 5 s
    c. 500 to 4000 rpm in 3 s (acceleration setting)
    d. hold at 4000 rpm for 40 s
6. Soft bake, 90 s @ 110 C; 5 minutes cool off (important before exposure to prevent wafer from sticking to mask)
7. Exposure energy: 28 mJ/cm2:
    a. 3.7 s exposure time with MNTL's Quintel (currently 7.5 mW/cm2 power output)
    b. 2.6 s exposure time with MNMS' Mask Aligner (currently 21.4 mW/cm2 power output)
8. Post Exposure Bake: 60 s @ 110 C (wafer directly on hotplate)
9. Develop in CD-26 for 18 s
    a. CD-26 underneath developer hood, on right
    b. Simply let wafer sit in developer (no agitation, swirling, etc.; this can cause features to break off of wafer)
10. Rinse in DI water for 2 minutes in a dish with DI water gently flowing into it or simply swirling the wafer gently in a static dish of DI water
11. Examine wafer under microscope.
12. Perform 20 s oxygen plasma on wafer(s) before placing in CHA for metal deposition
13. Evaporation: 250 Angstroms of titanium + 750 Angstroms of gold per wafer
14. Metal lift-off (do this in the biolab)

a. Place wafers in Remover PG at 70 C for 1 hour+
b. Dump liquid into non-halogenated solvent waste container
c. Wipe gently with a cleanroom wipe to remove any stubborn metal

Appendix B: Data acquisition scripts

Impedance spectroscopy measurements

```
clear all;
close all;

strResponse = input('Filename to save data?\n', 's');

tic;

%GPIB address
address = 20;

g = instrfind('Type', 'gpib', 'BoardIndex', 0, 'PrimaryAddress', address, 'Tag', '');
if isempty(g)
   g = gpib('NI', 0, address);
else
   fclose(g);
   g = g(1);
end
fopen(g);

fprintf(g,'FUNC:IMP ZTD')
fprintf(g,'VOLT 250 MV')

%4284A
%FREQ Array gives all frequency test values
frequencies = load('frequencies.mat','frequency');
scanthis = frequencies.frequency;

S = zeros(24,4);

%scan times:

fprintf('FREQUENCY,MAGNITUDE,PHASE (1)')
fprintf('\n')

for i = 1:24
   %Set FREQ
   FREQ = ['FREQ ' sprintf('%g', scanthis(i)) 'HZ'];
   fprintf(g,FREQ);
   pause(0.2)
   %FETCH
   fprintf(g,'FETCH?')
   f = fscanf(g);
   D = sscanf(f,'%f,%f,%f',[1,3]);
   %FREQ?
   fprintf(g,'FREQ?')
   f = fscanf(g);
   Q = sscanf(f,'%f');
```

```
   DISPLAY = [int2str(scanthis(i)) ',' int2str(D(1)) ',' int2str(D(2))];
   fprintf(DISPLAY)
   fprintf('\n')
   S(i,:) = [D Q];
end

fprintf('FREQUENCY,MAGNITUDE,PHASE (2)')
fprintf('\n')
for i = 1:24
   %Set FREQ
   FREQ = ['FREQ ' sprintf('%g', scanthis(i)) 'HZ'];
   fprintf(g,FREQ);
   pause(0.2)
   %FETCH
   fprintf(g,'FETCH?')
   f = fscanf(g);
   D = sscanf(f,'%f,%f,%f',[1,3]);
   %FREQ?
   fprintf(g,'FREQ?')
   f = fscanf(g);
   Q = sscanf(f,'%f');
   DISPLAY = [int2str(scanthis(i)) ',' int2str(D(1)) ',' int2str(D(2))];
   fprintf(DISPLAY)
   fprintf('\n')
   S2(i,:) = [D Q];
end

fprintf('FREQUENCY,MAGNITUDE,PHASE (3)')
fprintf('\n')
for i = 1:24
   %Set FREQ
   FREQ = ['FREQ ' sprintf('%g', scanthis(i)) 'HZ'];
   fprintf(g,FREQ);
   pause(0.2)
   %FETCH
   fprintf(g,'FETCH?')
   f = fscanf(g);
   D = sscanf(f,'%f,%f,%f',[1,3]);
   %FREQ?
   fprintf(g,'FREQ?')
   f = fscanf(g);
   Q = sscanf(f,'%f');
   DISPLAY = [int2str(scanthis(i)) ',' int2str(D(1)) ',' int2str(D(2))];
   fprintf(DISPLAY)
   fprintf('\n')
   S3(i,:) = [D Q];
end

fclose(g);
delete(g);
```

```
save(strResponse,'S','S2','S3');

toc

load('di_ref.mat');

hold on;
p = semilogx(di_ref(:,4),di_ref(:,1),'--');
p = semilogx(S(:,4),S(:,1));
p = semilogx(S2(:,4),S2(:,1));
p = semilogx(S3(:,4),S3(:,1));
set(gca,'XScale','log');
hold off;

figure;

hold on;
p = semilogx(di_ref(:,4),di_ref(:,2),'--');
p = semilogx(S(:,4),S(:,2));
p = semilogx(S2(:,4),S2(:,2));
p = semilogx(S3(:,4),S3(:,2));
set(gca,'XScale','log');
hold off;

pause(10);

close all;
```

Frequencies.mat

This file lists measurement frequencies and is called in the above script.

```
100
150
225
337.500000000000
506.250000000000
759.375000000000
1139.06250000000
1708.59375000000
2562.89062500000
3844.33593800000
5766.50390600000
8649.75585900000
12974.6337900000
19461.9506800000
29192.9260300000
43789.3890400000
65684.0835600000
98526.1253400000
```

147789.188000000
221683.782000000
332525.673000000
498788.509500000
748182.764300000
1000000

Real-time impedance measurements

```
clear all;
close all;

strResponse3 = input('Filename to starting sweep data?\n', 's');
strResponse = input('Filename to save time data?\n', 's');
strResponse2 = input('Filename to final sweep data?\n', 's');

%GPIB address
address = 20;

g = instrfind('Type', 'gpib', 'BoardIndex', 0, 'PrimaryAddress', address, 'Tag', '');
if isempty(g)
   g = gpib('NI', 0, address);
else
   fclose(g);
   g = g(1)
end
fopen(g);

fprintf(g,'FUNC:IMP ZTD')
fprintf(g,'VOLT 250 MV')

%4284A
%FREQ Array gives all frequency test values
frequencies = load('frequencies.mat','frequency');
scanthis = frequencies.frequency;

S = zeros(24,4);

%scan times:

for i = 1:24
   %Set FREQ
   FREQ = ['FREQ ' sprintf('%g', scanthis(i)) 'HZ'];
   fprintf(FREQ)
   fprintf('\n')
   fprintf(g,FREQ);
   pause(0.2)
   %FETCH
   fprintf(g,'FETCH?')
   f = fscanf(g);
   D = sscanf(f,'%f,%f,%f',[1,3]);
```

```
    %FREQ?
    fprintf(g,'FREQ?')
    f = fscanf(g);
    Q = sscanf(f,'%f');
    B(i,:) = [D Q];
end

save(strResponse3,'B');

semilogx(B(:,4),B(:,1));

figure;

semilogx(B(:,4),B(:,2));

fprintf(g,'FUNC:IMP ZTD')
fprintf(g,'VOLT 250 MV')


disp('Press enter to start time sweep');
pause;
disp('TIME SWEEP IN PROGRESS');

starttime = clock;

C = 0;
i = 1;
figure('Position',[0 0 1024 768]);

while C<5400
    %Set FREQ 2kHz
    FREQ = ['FREQ 2000 HZ'];
    fprintf(g,FREQ)
    pause(0.2)
    %FETCH
    fprintf(g,'FETCH?')
    f = fscanf(g);
    D = sscanf(f,'%f,%f,%f',[1,3]);
    %FREQ?
    fprintf(g,'FREQ?')
    f = fscanf(g);
    Q = sscanf(f,'%f');
    nowtime = clock;
    C = 60*60*(nowtime(4)-starttime(4))+60*(nowtime(5)-starttime(5))+nowtime(6)-starttime(6);
    A = nowtime;
    F(i,:) = [D Q C A];
    %Set FREQ 10kHz
    FREQ = ['FREQ 10000 HZ'];
    fprintf(g,FREQ)
    pause(0.2)
    %FETCH
```

```
    fprintf(g,'FETCH?')
    f = fscanf(g);
    D = sscanf(f,'%f,%f,%f',[1,3]);
    %FREQ?
    fprintf(g,'FREQ?')
    f = fscanf(g);
    Q = sscanf(f,'%f');
    nowtime = clock;
    C = 60*60*(nowtime(4)-starttime(4))+60*(nowtime(5)-starttime(5))+nowtime(6)-starttime(6);
    A = nowtime;
    G(i,:) = [D Q C A];
    %Set FREQ 100kHz
%     FREQ = ['FREQ 100000 HZ'];
%     fprintf(g,FREQ)
%     pause(0.2)
%     %FETCH
%     fprintf(g,'FETCH?')
%     f = fscanf(g);
%     D = sscanf(f,'%f,%f,%f',[1,3]);
%     %FREQ?
%     fprintf(g,'FREQ?')
%     f = fscanf(g);
%     Q = sscanf(f,'%f');
%     nowtime = clock;
%     C = 60*60*(nowtime(4)-starttime(4))+60*(nowtime(5)-starttime(5))+nowtime(6)-starttime(6);
%     A = nowtime;
%     H(i,:) = [D Q C A];
    subplot(2,1,1);
    plot(F(:,5),F(:,1),G(:,5),G(:,1));
    legend('2 kHz','10 kHz');
    ylabel('Impedance (\Omega)');
    xlabel('Time (s)');
    title('Impedance Magnitude in Real Time');
    if i>1
        diffF = diff(F(:,1))./diff(F(:,5));
        diffG = diff(G(:,1))./diff(G(:,5));
        subplot(2,1,2);
        plot(F(1:i-1,5),diffF,G(1:i-1,5),diffG);
        legend('2 kHz','10 kHz');
        ylabel('d\Omega/dt');
        xlabel('Time (s)');
        title('Impedance Magnitude in Real Time');
    end
    i = i+1;
    save(strResponse, 'F', 'G');
end

fprintf(g,'FUNC:IMP ZTD')
fprintf(g,'VOLT 250 MV')

%4284A
```

```
%FREQ Array gives all frequency test values
frequencies = load('frequencies.mat','frequency');
scanthis = frequencies.frequency;

S = zeros(24,4);

%scan times:

for i = 1:24
   %Set FREQ
   FREQ = ['FREQ ' sprintf('%g', scanthis(i)) 'HZ'];
   fprintf(FREQ)
   fprintf('\n')
   fprintf(g,FREQ);
   pause(0.2)
   %FETCH
   fprintf(g,'FETCH?')
   f = fscanf(g);
   D = sscanf(f,'%f,%f,%f',[1,3]);
   %FREQ?
   fprintf(g,'FREQ?')
   f = fscanf(g);
   Q = sscanf(f,'%f');
   S(i,:) = [D Q];
end

save(strResponse2,'S');

semilogx(S(:,4),S(:,1));

figure;

semilogx(S(:,4),S(:,2));

fclose(g);
delete(g);
```

Appendix C: Fitting protocol

Primary fitting script: fit_PCR.m

```
% Fit a certain function to measured impedance data
% Can choose to fit to mag-angle or real-imag
% Rafael Gomez 10/23/00 edited by Gregory Damhorst 3/22/13
clear all;
close all;
clc;

% Model
model = 'jacobs_PCR';

% Fit to mag-angle or real-imag?
% fmag = 1 --> mag-angle; fmag = 0 --> real_imag
fitmag = 1;

% First guess for parameters
% p0 = input('first guess of parameters:'); %jacobs
p0 = [1 10 1 1];

% Fix any parameters?
% Indexes of parameters to hold fixed
fixindex = [];
% Values of fixed parameters, corresponding to the indexes in fixindex
fixvalues = [];

% Plot only, no fit?
% If plotonly==1, data and model are plotted (with p0), but no fit is done
plotonly = 0;

% Accumulate figures?
accum = 1;

% Load data
fname = '../130215_imp_spec/130215_A2.mat';
savename = '../130215_imp_spec/130323_fit_A2.mat';
load(fname);
%data is in S

% Column 1 is frequency
freq = 2*pi*S(:, 4);
data(:,1) = freq; %just in case
% Column 2 is impedance magnitude
data(:,2) = S(:,1);
% Column 3 is impedance angle
data(:,3) = S(:, 2)*pi/180;
% Fourth column is Real(Z)
data(:, 4) = data(:, 2).*cos(data(:, 3));
% Fifth column is Imag(Z)
```

```
data(:, 5) = data(:, 2).*sin(data(:, 3));

% Frequency range to fit
rng = 1:24;

% Select kind of data to fit
z = zeros(length(rng), 2);
if fitmag
  % Mag-angle
        z(:, 1) = log(data(rng, 2));
        z(:, 2) = data(rng, 3);
else
  % Real-imag
  z(:, 1) = log(data(rng, 4));
  z(:, 2) = log(data(rng, 5));
end;

% Display settings
disp(['File: ' fname]);
disp(['Model: ' upper(model)]);
if fitmag
   disp('Fitting to MAGNITUDE-ANGLE');
else
   disp('Fitting to REAL-IMAGINARY');
end

% These two lines eliminate the need for jacob_pcr_info.m
parnames = {'Rsol', 'C_di', 'n', 'B'};
parunits = {'kOhm', 'pF', 'x1e-2', 'x1e-10'};

numpars = length(parnames);
disp(['Freq. range: ' num2str(data(rng(1), 1), '%5.4e') ' Hz to '  num2str(data(rng(end), 1), '%5.4e') ' Hz']);
disp('First guess of parameters:');
[snames, sunits, svalues] = fmt_params(parnames, parunits, p0);
disp(snames);
disp(sunits);
disp(svalues);

% Upper bounds
pupp = inf*ones(size(p0));
% Lower bounds
plow = 1e-10*ones(size(p0));

p = p0;
if ~plotonly
  tolfun = 1e-10;
        for ii = 1:2
    opt = optimset('TolX', 1e-12, 'MaxFunEvals', 1000000, 'TolFun', tolfun, ...
      'MaxIter', 1000000, 'LargeScale', 'on', 'Display', 'on');
                [p, residue] = lsqcurvefit(model, p0, freq(rng), z, plow, pupp, opt, fitmag, fixindex,
fixvalues);
```

```
      p0 = p;
  tolfun = tolfun/1000;
   end;
end;

if ~plotonly
    % Display results from fit
    disp('  ');
    disp('Parameters from fit:');
    [snames, sunits, svalues] = fmt_params(parnames, parunits, p0);
    disp(snames);
    disp(sunits);
    disp(svalues);
    disp(' ');
    disp(['Residue per point from lsqcurvefit: ' num2str(residue/length(rng), '%5.4e') ' (' int2str(length(rng))
' points)']);
end

%w = logspace(2.6, 7, 100)';
w = freq;
zfit = zeros(length(w), 4);
if fitmag
            zfit(:, 1:2) = feval(model, p, w, fitmag, fixindex, fixvalues);
            zfit(:, 1) = exp(zfit(:, 1));
            zfit(:, 3) = zfit(:, 1).*cos(zfit(:, 2));
            zfit(:, 4) = zfit(:, 1).*sin(zfit(:, 2));
else
   zfit(:, 3:4) = exp(feval(model, p, w, fitmag, fixindex, fixvalues));
   zcomp = zfit(:, 3) + i*zfit(:, 4);
   zfit(:, 1) = abs(zcomp);
   zfit(:, 2) = angle(zcomp);
end;

if ~plotonly
    % Calculate residues from real-imag
    res_ri = sum((log(data(:, 4)) - log(zfit(:, 3))).^2) + sum((log(data(:, 5)) - log(zfit(:, 4))).^2);
    % Calculate resides from mag-angle
    res_ma = sum((log(data(:, 2)) - log(zfit(:, 1))).^2) + sum((data(:, 3) - zfit(:, 2)).^2);
    disp(['Residue per point (real-imag): ' num2str(res_ri/length(rng), '%5.4e') ' (' int2str(length(rng)) '
points)']);
    disp(['Residue per point (mag-angle): ' num2str(res_ma/length(rng), '%5.4e') ' (' int2str(length(rng)) '
points)']);
    disp('');
    disp(['Total residue per point (r-i + m-a): ' num2str((res_ri + res_ma)/length(rng), '%5.4e') ' ('
int2str(length(rng)) ' points)']);
end

tit = ['Fit to ', fname, '  with ', model];
if 1
   if accum
      fh = figure;
```

```
  else
    fh = figure(1);
  end;
%   set(fh, 'position', [200 430 750 500]);
%   set(fh, 'PaperPosition', [0.83 3.28 6.84 4.44]);
  subplot(2, 1, 1);
          ph = [];
  ph = [ph loglog(data(:, 1)/(2*pi), abs(data(:, 4)), 'k+', w/(2*pi), abs(zfit(:, 3)))];
  set(ph, 'MarkerSize', 10);
  th = title(tit);
  set(th, 'Interpreter', 'none');
  xlabel('Frequency [Hz]');
  ylabel('Real(Z) [{\Omega}]');
  %legend('Measured', 'Fitted model');

  subplot(2, 1, 2);
  ph = [ph loglog(data(:, 1)/(2*pi), abs(data(:, 5)), 'k+', w/(2*pi), abs(zfit(:, 4)))];
  set(ph, 'MarkerSize', 10);
  xlabel('Frequency [Hz]');
  ylabel('Imag(Z) [{\Omega}]');
%   plformat(fh, ph, 14);
  legend( 'Measured', 'Fitted model');
end

if 1
  if accum
    fh = figure;
  else
    fh = figure(2);
  end;
%   set(fh, 'position', [250 380 750 500]);
%   set(fh, 'PaperPosition', [0.83 3.28 6.84 4.44]);
          ph = [];
  subplot(2, 1, 1);
  ph = [ph loglog(data(:, 1)/(2*pi), data(:, 2), 'k+', w/(2*pi), zfit(:, 1))];
  set(ph, 'MarkerSize', 10);
  th = title(tit);
  set(th, 'Interpreter', 'none');
%    axis([20 1e6 0 1E9]);
          xlabel('Frequency [Hz]');
  ylabel('Impedance Magnitude [{\Omega}]');

  subplot(2, 1, 2);
  ph = [ph semilogx(data(:, 1)/(2*pi), data(:, 3)*180/pi, 'k+', w/(2*pi), zfit(:, 2)*180/pi)];
  set(ph, 'MarkerSize', 10);
%    axis([20 1e6 -90 0]);
  xlabel('Frequency [Hz]');
  ylabel('Angle [Deg]');
%   plformat(fh, ph, 14);
  legend( 'Measured', 'Fitted model');
end
```

```
f = w/(2*pi);
save(savename,'f','zfit','snames','sunits','svalues');
```

Function: *fmt_params*

```
function [snames, sunits, svalues] = fmt_params(parnames, parunits, par);
% FMT_PARAMS Returns strings with the formatted parameters, for printing
%
% [snames, sunits, svalues] = fmt_params(parnames, parunits, par)
%
%    parnames = Cell array of strings with names of parameters
%    parunits = Cell array of strings with units of parameters
%    par = Vector with values of parameters
%
%    snames = String with formatted names of paramaters
%    spares = String with formatted names of paramaters
%    svalues = String with formatted values of paramaters
%
% R. Gomez 8/3/02

% Build arrays with names and units fo parameetrs
numpars = length(parnames);
snames = '    ';
sunits = '    ';
svalues = 'p = ';
dummy = '                                        ';
for ii = 1:numpars
   vv = num2str(par(ii), '%5.4e');
   ln = length(parnames{ii});
   lu = length(parunits{ii});
   lv = length(vv);
   lmax = max([ln lu lv]) + 2;
   tmp = dummy(1:(lmax-ln));
   snames = [snames parnames{ii} tmp];
   tmp = dummy(1:(lmax-lu));
   sunits = [sunits parunits{ii} tmp];
   tmp = dummy(1:(lmax-lv));
   svalues = [svalues vv tmp];
end
```